Graduate School Form
30 Updated 12/26/2015

PURDUE UNIVERSITY
GRADUATE SCHOOL
Thesis/Dissertation Acceptance

This is to certify that the thesis/dissertation prepared

By Hanyin Zhang

Entitled

CHARACTERIZATION OF TENSILE, CREEP, AND FATIGUE PROPERTIES OF 3D PRINTED ACRYLONITRILE BUTADIENE STYRENE

For the degree of Master of Science in Mechanical Engineering

Is approved by the final examining committee:

Jing Zhang
Chair

Alan Jones

Jong Eun Ryu

To the best of my knowledge and as understood by the student in the Thesis/Dissertation Agreement, Publication Delay, and Certification Disclaimer (Graduate School Form 32), this thesis/dissertation adheres to the provisions of Purdue University's "Policy of Integrity in Research" and the use of copyright material.

Approved by Major Professor(s): Jing Zhang

Approved by: Sohel Anwar 7/22/2016

Head of the Departmental Graduate Program Date

CHARACTERIZATION OF TENSILE, CREEP, AND FATIGUE PROPERTIES OF 3D PRINTED ACRYLONITRILE BUTADIENE STYRENE

A Thesis

Submitted to the Faculty

of

Purdue University

by

Hanyin Zhang

In Partial Fulfillment of the

Requirements for the Degree

of

Master of Science in Mechanical Engineering

August 2016

Purdue University

Indianapolis, Indiana

ACKNOWLEDGMENTS

First, I would like to thank my advisor and committee chairman, Dr. Jing Zhang, for his invaluable guidance which helped me in realizing this research throughout the course of my studies.

I also would like to extend my special thanks to Dr. Jing Zhang for giving me the opportunity to work on this research project, and also Mr. Weng Hoh Lee for discussing about thesis research and writing; and to Dr. Jong Eun Ryu and Dr. Alan Jones for serving on my thesis committee and giving me abundant suggestion for thesis work.

I am grateful for valuable assistance from Michael Golub for providing me the opportunity to use the facilities of the Machine Shop, and Ms. Linlin Cai and Mr. Joseph Derrick for generously providing creep test model, and assisting with creep test.

Finally, I would thank to my parents and Fei, without them, none of this would have been possible.

TABLE OF CONTENTS

Page

LIST OF TABLES

LIST OF FIGURES

Figure Page

Figure Page

ABSTRACT

Zhang, Hanyin. M.S.M.E, Purdue University, August 2016. Characterization of Tensile, Creep, and Fatigue Properties of 3D Printed Acrylonitrile Butadiene Styrene. Major Professor: Jing Zhang.

Acrylonitrile Butadiene Styrene (ABS) is the most widely used thermoplastics in 3D printing for making models, prototypes, patterns, tools and end-use parts. However, there is a lack of systematic understanding of the mechanical properties of 3D printed ABS components, including orientation-dependent tensile strength, creep, and fatigue properties. These mechanical properties are critically needed for design and application of 3D printed components.

The main objective of this research is to systematically characterize key mechanical properties of 3D printed ABS components, including tensile, creep, and fatigue properties. Additionally, the effects of printing orientation on the mechanical properties are investigated. There are two research approaches employed in the thesis: first, experimental investigation of the tensile, creep, and fatigue properties of the 3D printed ABS components; second, laminate based finite-element modeling of tensile test to understand the stress distributions in different printing layers.

The major conclusions of the thesis work are summarized as follows. The tensile test experiments show that the 0 ° printing orientation has the highest Youngs modulus, 1.81 GPa, and ultimate strength, 224 MPa. The tensile test simulation shows a similar Youngs modulus as the experiment in elastic region, indicating the robustness of laminate based finite element model. In the creep test, the 90 ° printing orientation has the lowest k value of 0.2 in the plastics creep model, suggesting the 90 ° is the most creep resistant among 0 °, 45 °, and 90 ° printing orientations. In the fatigue test, the average cycle number under load of 30 N is 3796 revolutions.

The average cycle number decreases to 128 revolutions when the load is below 60N. Using the Paris Law, with the crack size of 0.75 mm long and stress intensity factor is varied from 352 to 700 $MN - m^{\frac{3}{2}}$, the predicted fatigue crack growth rate is 0.0341 mm/cycle.

Key words: Acrylonitrile Butadiene Styrene (ABS); additive manufacturing; 3D printing; printing orientation; tensile; creep; fatigue; finite element

1. INTRODUCTION

1.1 Background

Three dimensional (3D) printing is a technique of rapid prototyping, which uses a digital document created by the physical model, then constructs the object layer by layer with powder metal or plastic material filament. 3D printing usually uses digital technology to achieve the printing order, compared to the traditional mold manufacturing, which involved complex industrial design and other time-consuming technologies [1]. 3D printing technology is based on a 3D computer design model created by designated software, and uses a laser beam or melt nozzle to fuse special materials like metal powder, ceramic powder, plastic, etc. Then those melted materials will be stacked and bonded layer by layer. Eventually, by the precise movement of nozzle and laser beam, the physical product will generate from digital codes. Since the 3D printer reads the model file by layers, this feature enables its technology to create almost any shape of objects.

In contrast with traditional manufacturing industries which use cutting, molding, milling, and other machining methods on raw materials in order to achieve final production, 3D printing technology can greatly reduce the complexity of manufacturing by slicing a 3D entity into numbers of layers of two-dimensional planes, then superimposing them on the material handling and production. 3D printing technology can directly generate any shape from the computer graphics data without requiring a complex digital manufacturing process, huge machines, and a vast amount of manpower. Therefore, production can easily be manufactured by more people. There are various forms of orientation to stack each layer. Some 3D printers use ink-jet approach. For example, a company called Objet from Israel uses the printer-head to spray very thin layer of liquid plastic material on the mold tray, then the coating

will be placed under ultraviolet light for processing. The mold tray will fall a slight distance for the next layer stack up. Also a company called Stratasys, uses fused deposition modeling technology, which the entire process is melting plastic in the nozzle, and then depositing a thin layer of plastic.

Some 3D printing systems use powders as printing materials. The particles are sprayed on the mold tray to form a very thin layer of powder layer, and then cured by the discharge of the liquid adhesive. There also use a technique called laser sintering technology which cast laser on raw powder material to form predetermined shape. This technology has been used by a German company called EOS GmbH Electro Optical Systems. Also, the Swiss company Arcam using electron current to melt the powder particles in a vacuum condition. These different technologies mentioned above are only several of many ways used in current fast growing industries. When facing a complex structure contains holes or bridges, gluing gels or other substances will be needed to provide support or occupy spaces in between particles. This part of the powder will not be casted, but will need to be rinsed off with water or compressed air. Today, 3D printing can be used to print a wide variety materials from a different kinds of plastics, metals, ceramics and rubber-like substance. Some printers can be combined in different materials, in order to print out a hard object while some part of it remain soft.

Additive manufacturing involves a process from creating a CAD model to printing a part. The first step always involves converting external geometry into a professional CAD solid-modeling software. After finishing the CAD modeling, the 3D profile needs to be converted to an STL file, which essentially describes the small steps of how the printer is going to move. Next step is to properly set up the machine before it starts printing; the settings include material constraints, timing, etc. After the model has been printed, it can be removed and cleaned up before it is ready to be used.

The thickness of printing section (Z direction) and the resolution of planar direction (X-Y plane) are calculated by microns (1×10^{-6} meter) and DPI (pixels per inch). The general layer thickness is around 100 microns, or 0.1 millimeters. Some

more advanced, precise printers, such as Objet Connex from Stratasys and Pro-Jet from 3D Systems series, can print out a thin layer of 16 microns [2]. Using traditional methods to create a model usually takes several days, depending on the size and complexity of the model. However, 3D printing technology can shorten the time to several hours; of course, the size and complexity of the performance of the printer may add printing time. Traditional manufacturing techniques such as injection molding can be mass-produced with low cost polymer products, in contrast with 3D printing technology which can be faster, more flexible and more cost-effective way to produce a relatively small number of products.

3D printing technology can process more complex parts than traditional methods [1]. A conventional manufacturing method usually starts from a raw block of materials, then cuts out unwanted areas. Another traditional method creates a mold, then fills it with melted metal or plastic. 3D printing technology has great advantages in terms of creating complex parts, which also reduce the manufacturing time. Secondly, 3D printing can form the model all at once, which means after-treatment is greatly reduced. This can avoid data leaks and shorten the outsourcing time span, which is important for the high-security industries such as defense or nuclear power. Again due to the significant reduction in manufacturing preparation and data conversion time, single experimental production cycle and small batch production costs are decreased, which is favorable for the development of new products. High speed and ease of use are helping 3D printing become a new trend in many fields, including architectural design, industrial modeling, and animation [3].

1.2 Objective of Thesis

The objective of this research is to systematically characterize the key mechanical properties of 3D printed Acrylonitrile-Butadiene-Styrene (ABS), including tensile, creep, and fatigue. Additionally, the effects of printing orientation on the mechanical properties are investigated. The mechanical property data are critically needed by the community for adopting the 3D printing technique for their specific applications.

With this objective in mind, the specific aims of the work include: (1) experimental investigation of tensile, creep, and fatigue properties of the 3D printed ABS; (2) development of a finite-element based computational model to simulate tensile testing, and understand stress distribution in different layers.

1.3 Problem Statement

3D printing technology can seamlessly print products, and its stability and strength of the connection between the structures much higher than traditional methods. However the material properties are very depending on the printing method and orientation. In this research, Fused Deposition Modeling (FDM) technique is the main method to print test specimen [4]. FDM uses a hot melting nozzle, therefore, that the melted materials will be extruded, deposited, molded layer by layer according to the path defined by computer-controlled program [5]. After deposition and coagulation, support material can be removed, in order to give the desired 3D product. The raw material used by FDM is generally a thermoplastic polymer include Acrylonitrile-Butadiene-Styrene (ABS), Polylactic acid, poly-amide, polyester, etc. ABS plastic is a widely used in FDM printing, where acrylonitrile can provide chemical resistance and impact resistance, butadiene is to provide toughness and impact resistance, styrene imparting rigidity and easy post-processing. Because ABS has become a common raw material 3D printing because of its various advantages, including heat resistance, low-temperature-impact resistance, glossy surface, easy coloring. The

other commonly used 3D printing material is PLA, which is stronger than ABS, but more brittle [6].

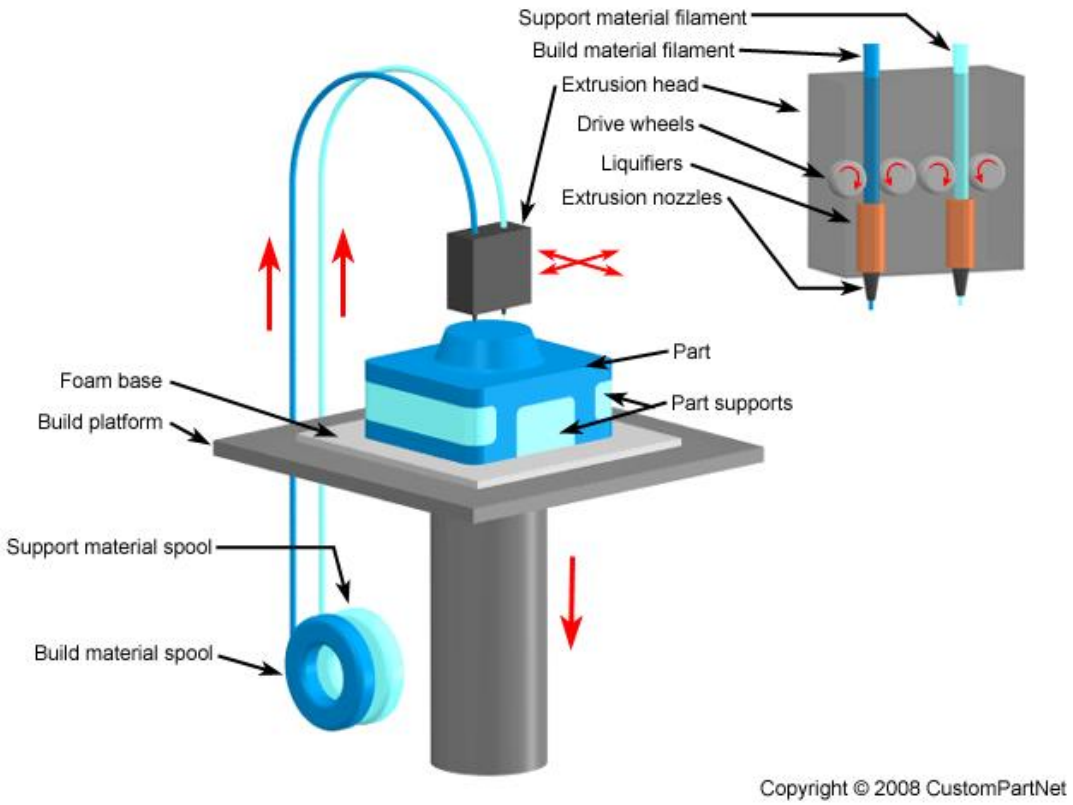

Fig. 1.1. Fused Deposition Modeling (FDM) System [7]

For Fused Deposition Modeling, its product strength is anisotropic. Depending on the load direction of printing, design, and stacking direction of layers, both should be considered as a variable to material strength. For example, the most basic rule is to avoid letting prints withstand shear stress in the stacking direction, since the shear stress load tolerance is relatively small [8].

1.4 Structure of Thesis

This thesis is organized into six chapters provide a clear and logical flow of content. The first chapter is an introduction of thesis work, giving the background of research, a statement of the current problem and objective of this thesis.

Chapter 2, Chapter 4, and Chapter 5 provides information about materials used, printing process, test method, research data and correlated graphs of three different approaches, tensile test, creep test and fatigue test. Chapter 3 investigates the tensile test with numerical method, including governing equations, CAD geometry, material model, boundary conditions and ANSYS analysis. Last but not least, Chapter 6 gives conclusions and directions of future study.

2. TENSILE TEST

2.1 Experimental Details

2.1.1 Materials

The specimens used in this study are designed in accordance with the ASTM standard test method for tensile properties of plastics [9]. The printer used is a Dimension SST 3D printer in conjunction with CatalystEx software, both products of Stratasys Inc. The 3D printed specimen material used is ABS, also a product of Stratasys Inc.

2.1.2 Printing Process

Fused deposition modeling is the 3D printing technique used to fabricate tensile test specimens. First, drawn a CAD model from a solid modeling software by using measured data of the physical model, then slice the CAD model with the data processing software which compiled into a bulk scan NC program. Secondly, numerical control commands controls the motion of heated nozzle, which orderly deposit melted materials on a layer of sheet, including border outline and fill scan contours. After the completion of a stacked layer, printing platform descend one layer height, and then continue to deposit next layer. The printing process will finish till the completion of the accumulation of superimposed layers forming the whole entity. Print parameters through optimized as follows: melting temperature in a range of 220 °C to 230 °C, the nozzle diameter of 0.5 mm, the print speed of 30 mm/s, layer height 0.1 mm, internal contour with 100% dense packing accumulation mode. Those parameter play important roles in tensile test [10], however, only the printing orientation is focused on this research.

2.1.3 Test

First, prepare the specimen, measure the width and length of the specimen in the perpendicular directions, and then choose the average number to calculate original cross-sectional area of the specimen A. Secondly, adjust the testing machine based on the maximum load and the tensile strength of the ABS plastic, configure the extensometer, and select the appropriate measurement portion. Turn on the testing machine, so that the table rises about 10mm, to eliminate the influence of the weight influence. Then, clamp the specimen to both sides of the machine. After that, inspect the tensile machine. In order to check whether the test is working properly, start testing machine, place a small amount of pre-load, and then unloaded to zero. Start the experiment, the tensile strain rate applied is 0.0847 mm/s. Observe the yield phase slippage and necking phenomenon when extension of specimen reaches the maximum. The machine stops immediately when specimen break, then the maximum load value will be recorded. The MTS software will record a raw data which can be organized in Microsoft Excel [11].

Fig. 2.1. Tensile Specimen Tested in the MTS Testing Machine

In this research, three different printing orientation are being tested: 0°, 45°, and 90° (Figure 2.2). 0° refer as the specimen print along the x-axis. 45° refer as the specimen placed in between x-axis and y-axis. By the contrast, 90° printing orientation refers the specimen prints along the y-axis. Printing orientation defines how an object is printed on the platform, which eventually can affect the strength and other properties of the object [12]. Stratasys can optimize the orientation of each layers once the model file is imported in it.

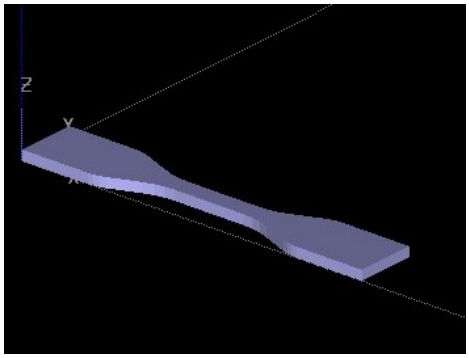

(a) 0 °

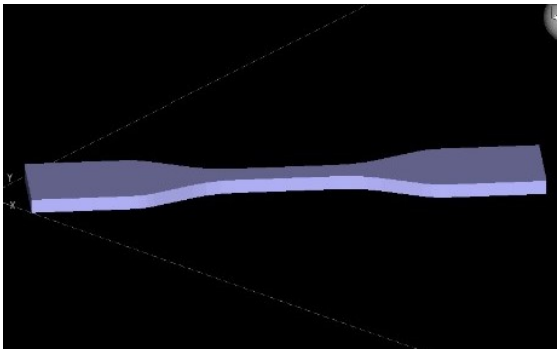

(b) 45 °

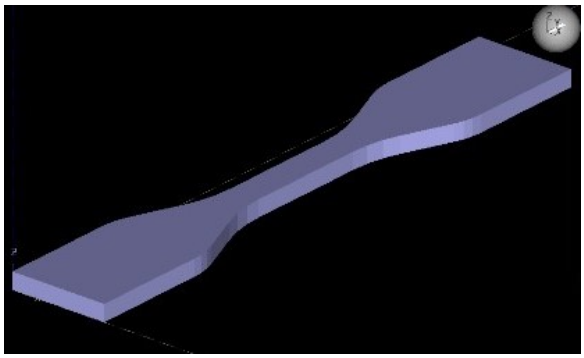

(c) 90 °

Fig. 2.2. Printing Orientations of the Tensile Specimens (a) 0 °, (b) 45 °, and (c) 90 °

Stratasys allows users to define how the object being printed on the platform. The 135 ° printing orientation example from Figure 2.3 to Figure 2.12 show how each layer has a different orientation than how the object being placed on the platform. Table 2.1 shows how each layer is angled differently among 0 °, 45 °, and 90 ° printing orientation. After collecting each layer orientation, a frequency chart (Figure 2.13) was created to illustrate the layer angles repeating about every five layers.

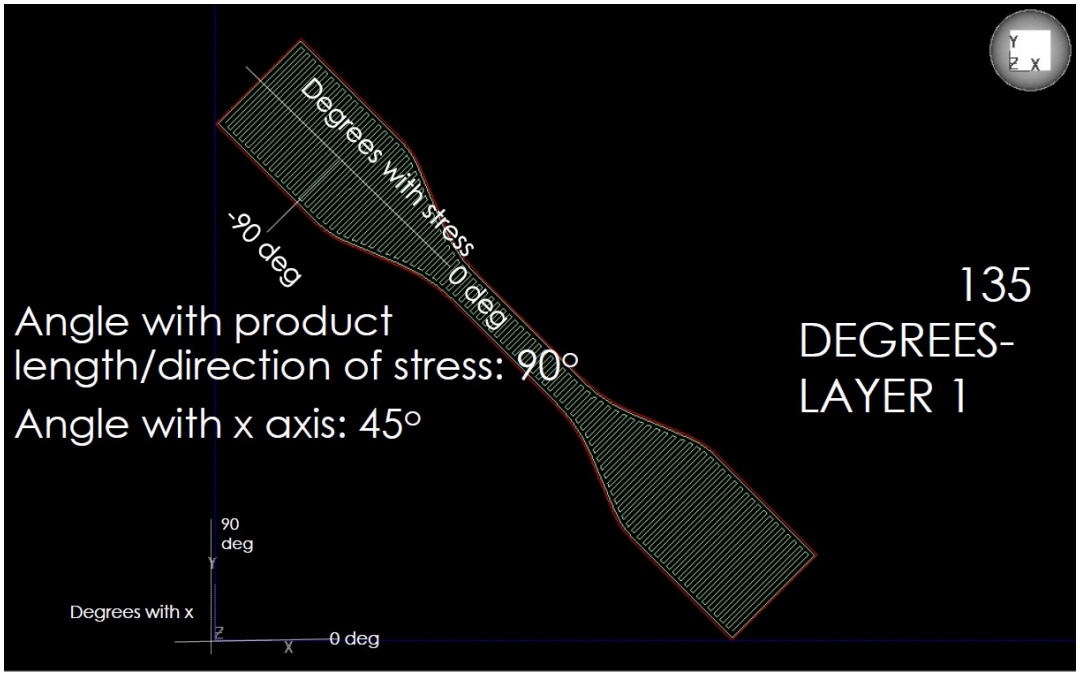

Fig. 2.3. Angle with Stress verses 135° Printing Orientation - Layer 1

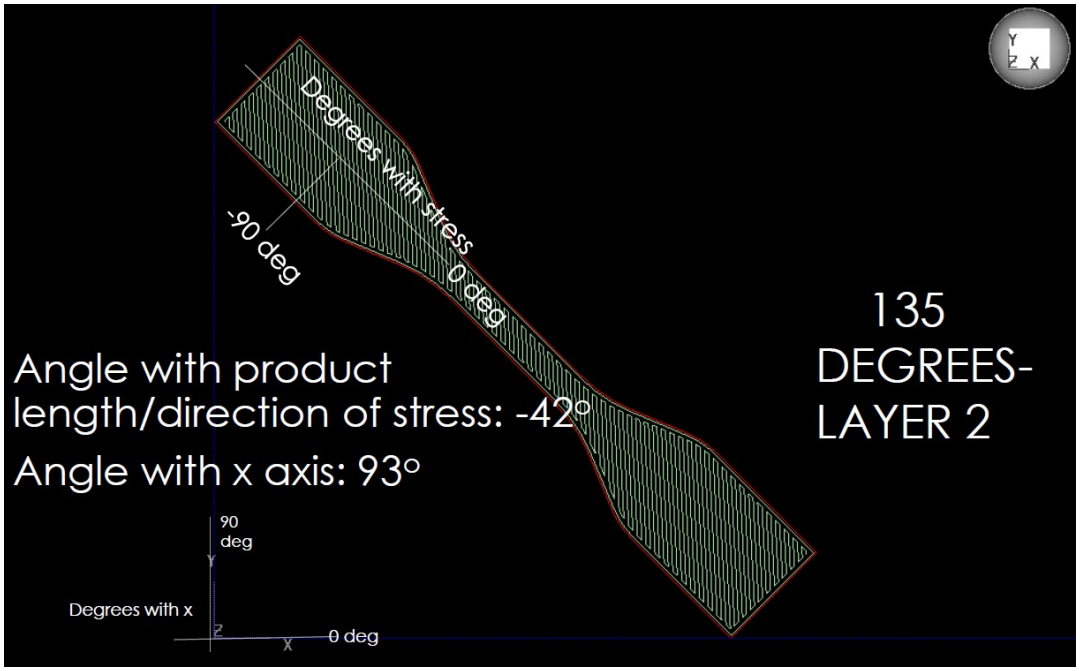

Fig. 2.4. Angle with Stress verses 135° Printing Orientation - Layer 2

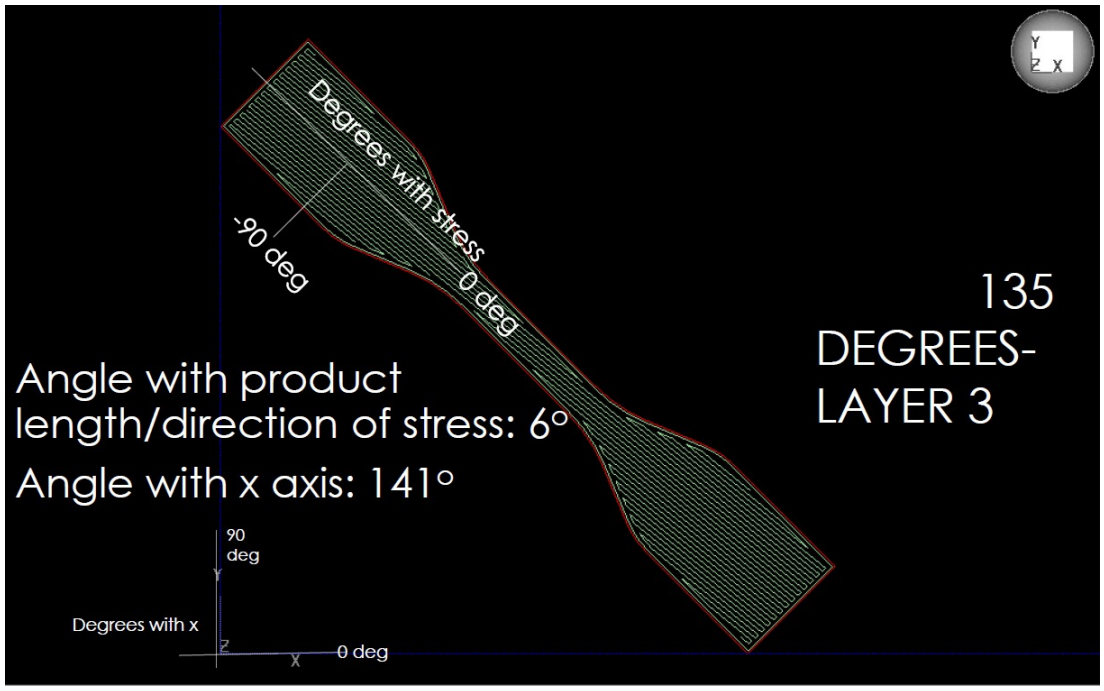

Fig. 2.5. Angle with Stress verses 135° Printing Orientation - Layer 3

Fig. 2.6. Angle with Stress verses 135° Printing Orientation - Layer 4

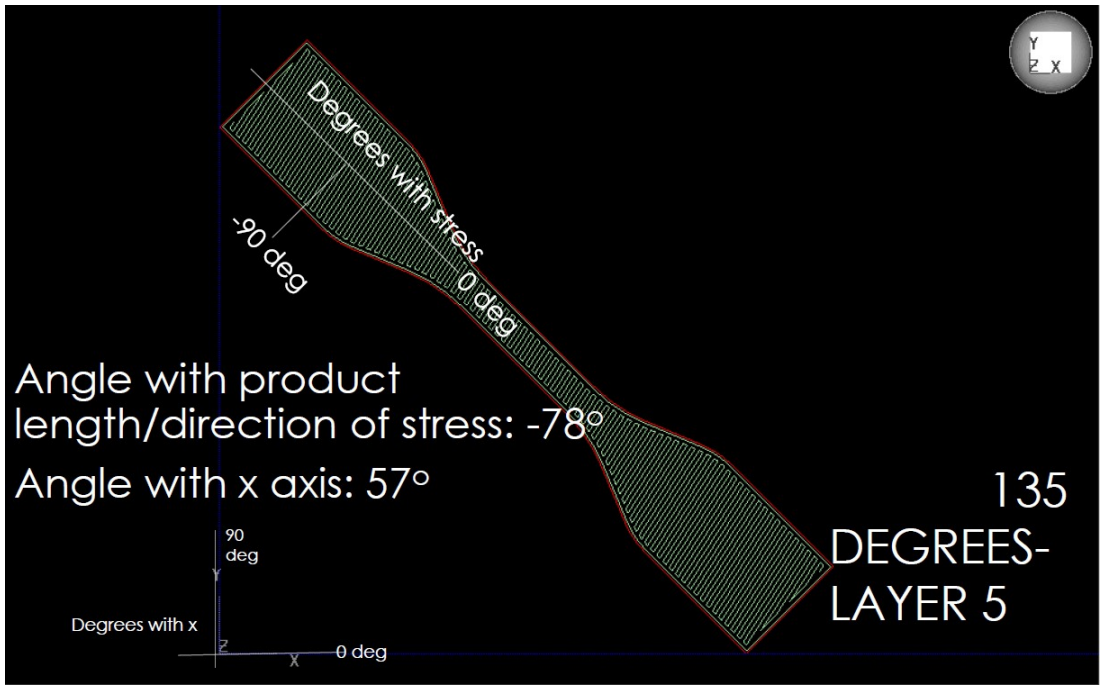

Fig. 2.7. Angle with Stress verses 135° Printing Orientation - Layer 5

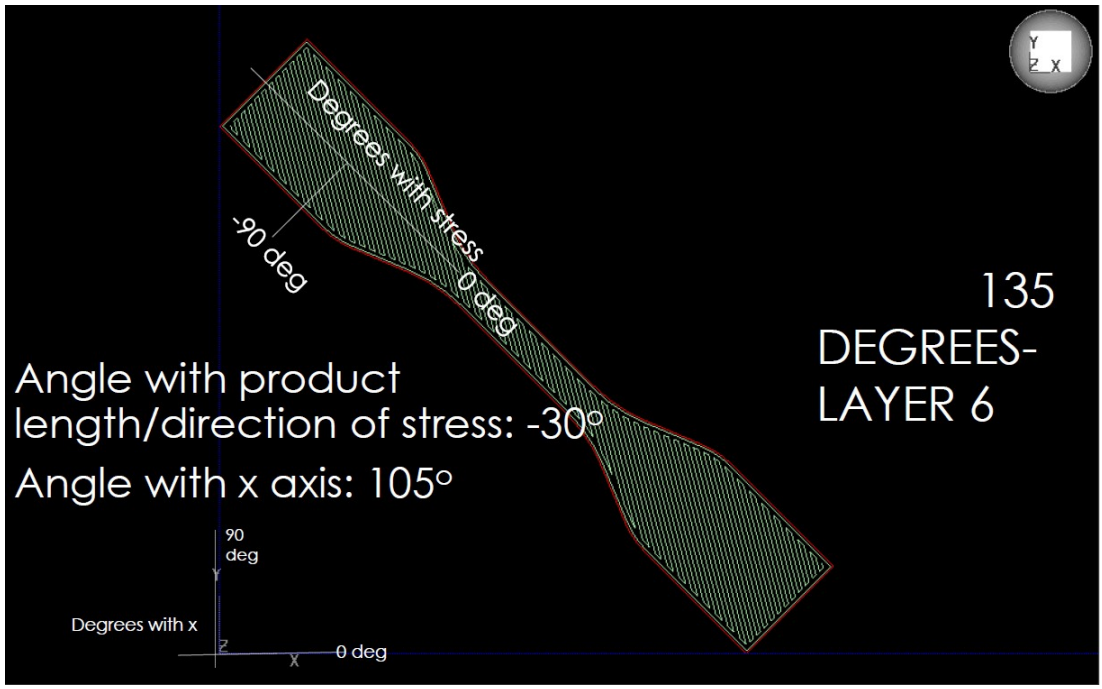

Fig. 2.8. Angle with Stress verses 135° Printing Orientation - Layer 6

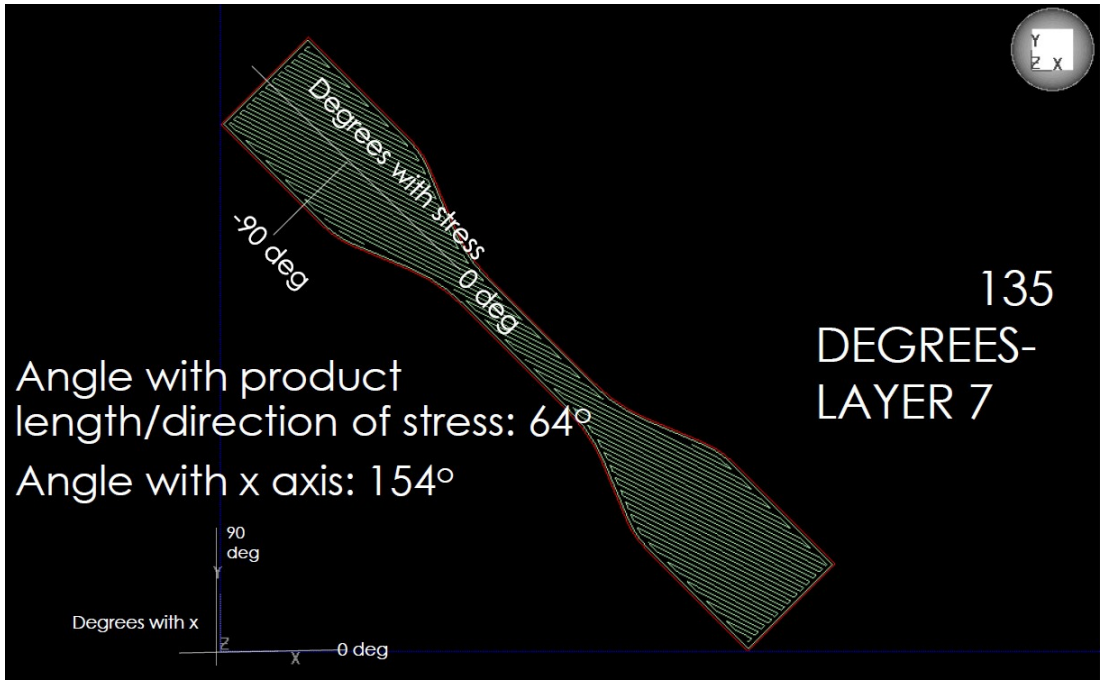

Fig. 2.9. Angle with Stress verses 135 ° Printing Orientation - Layer 7

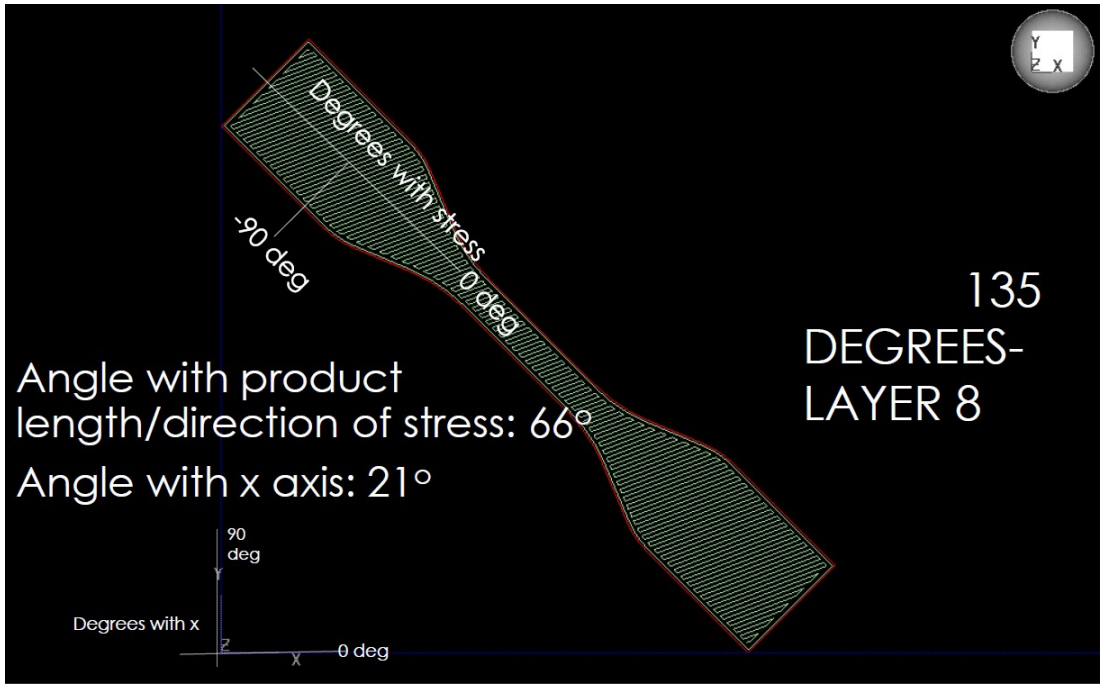

Fig. 2.10. Angle with Stress verses 135 ° Printing Orientation - Layer 8

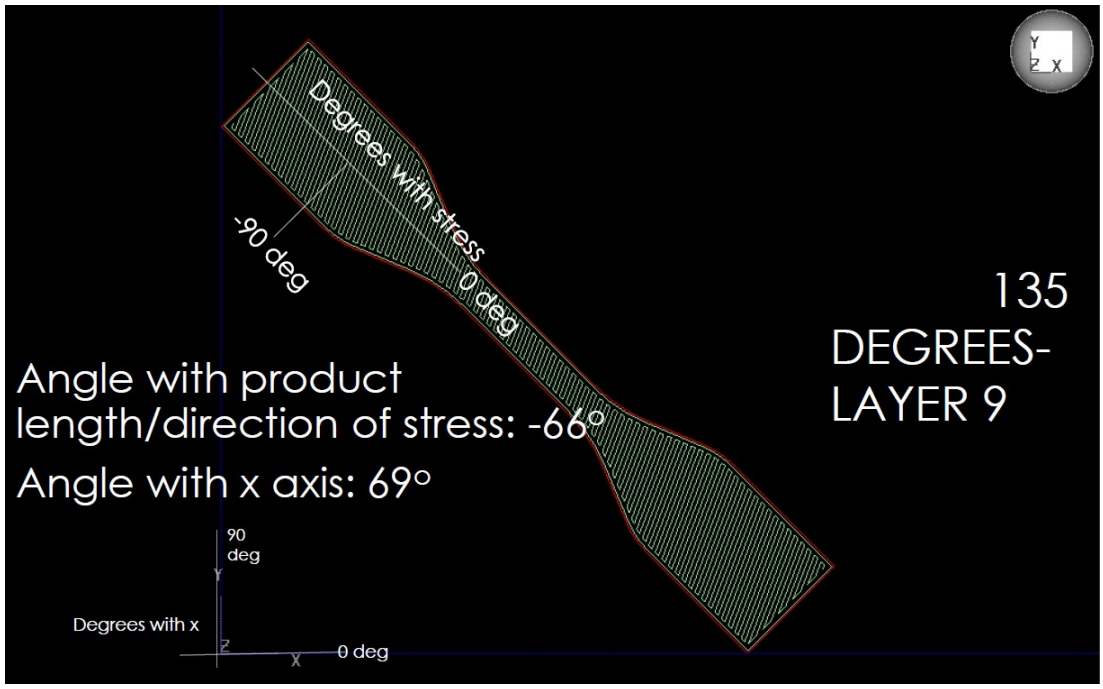

Fig. 2.11. Angle with Stress verses 135° Printing Orientation - Layer 9

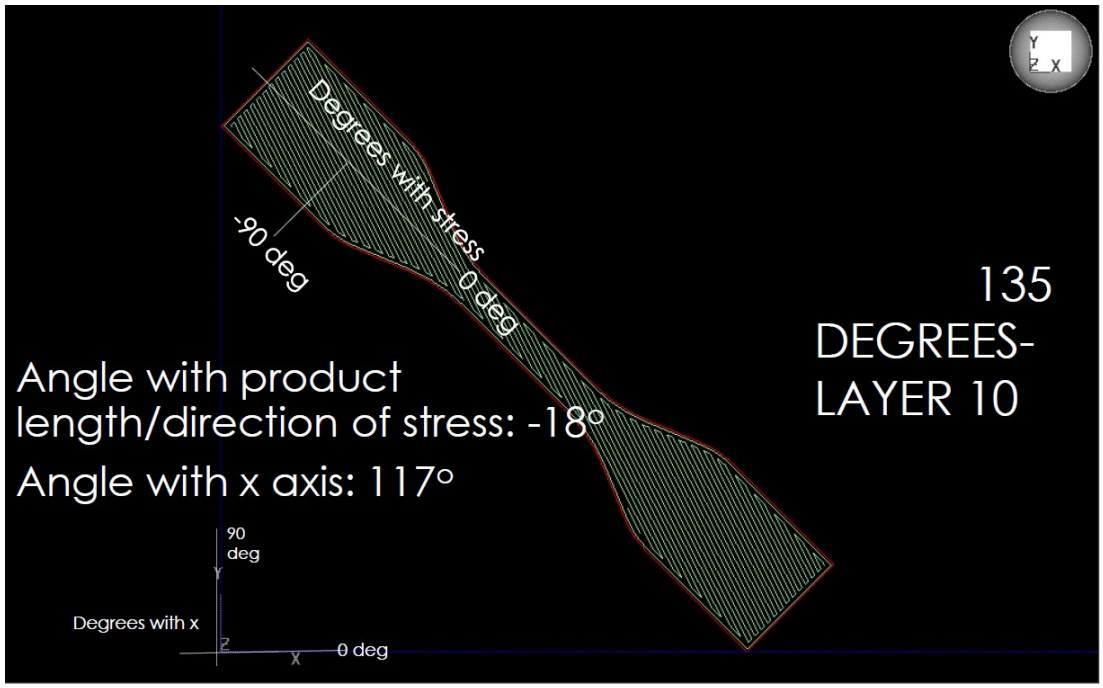

Fig. 2.12. Angle with Stress verses 135° Printing Orientation - Layer 10

Table 2.1
Degrees from Stress Axis and Degrees from X-Axis

	Printing Orientation		
	0°	45°	90°
Layer #	**Degrees of each layer from Stress axis**		
1	45	0	-45
2	-88	48	5
3	-38	-84	51
4	9	-37	-79
5	57	12	-33
6	-75	60	18
7	-27	-71	62
8	21	-25	-69
9	69	35	-21
10	-68	71	28

From Figure 2.13, we can see that the degrees of each layer from stress axis is forming a sin wave with 2π period.

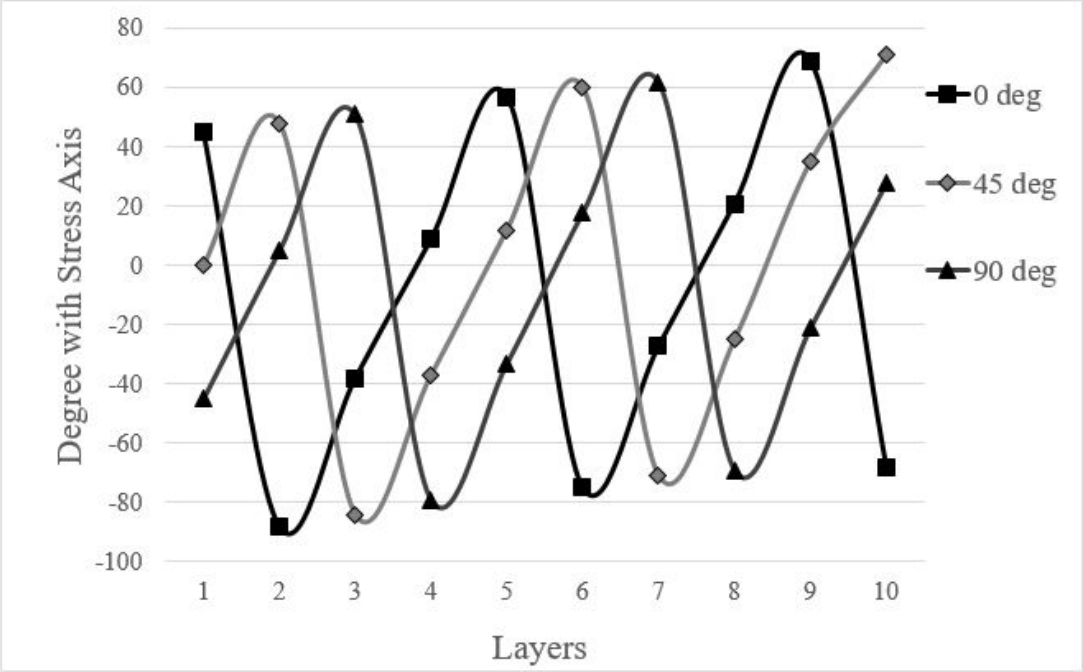

Fig. 2.13. Layer Orientation Difference with Stress Axis

2.2 Results and Discussion

Figure 2.14 shows the 0° printed tensile bar sample before and after the tensile test. The breaking gap is slightly above the center, but it still inside of the range of extensometer. Reasons why the tensile bar is not broken in the center will be discussed in Chapter 3.

The detailed cross sectional view of the fracture surface is given in Figure 2.15. It is very clear to see each layer from layer 1 to layer 10. When each layer was being built, the printer automatically printed an enclosure of the border.

(a) (b)

Fig. 2.14. Optical Images of 0 ° Tensile Bar (a) Before and (b) After Tensile Test

The stress-strain curves of tensile bars in different printing orientations are plotted in Figure 2.17. This figure shows a brittle material characteristic, which 0 ° printing orientation has higher ultimate stress and yielding stress compare 45 ° and 90 ° printing orientation. As shown in Table 2.2, the Youngs modulus for the 0 °, 45 °, and 90 ° orientations are 1.81 GPa, 1.80 GPa, and 1.78 GPa, respectively. A study shows the 0 ° has the advantage on tensile properties among printing flat, edge and upright [13].

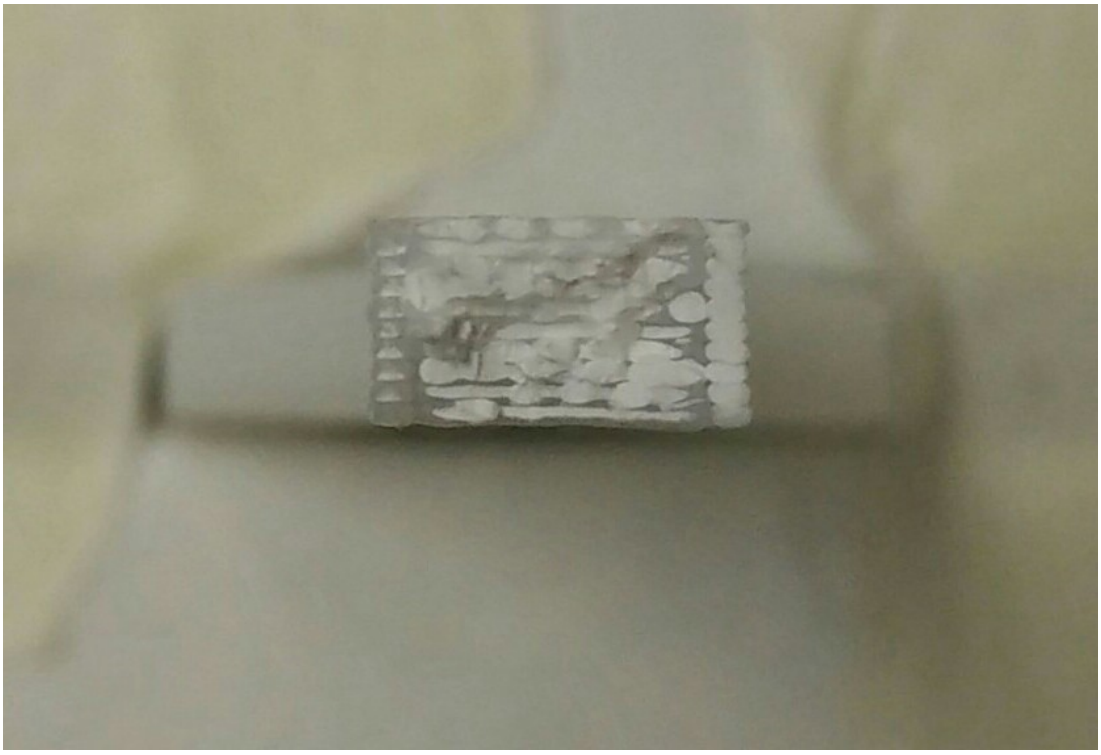

Fig. 2.15. Optical Image of Cross-Section Area of the 0 ° Tensile Bar Fracture Surface

Table 2.2
Averaged Mechanical Strength as a Function of Printing Orientation

Printing Orientation	0 °	45 °	90 °
Young's Modulus (GPa)	1.81+/-0.10	1.80+/-0.11	1.78+/-0.13
Ultimate Strength (MPa)	22.4+/-0.1	20.7+/-0.1	19.0+/- 0.2

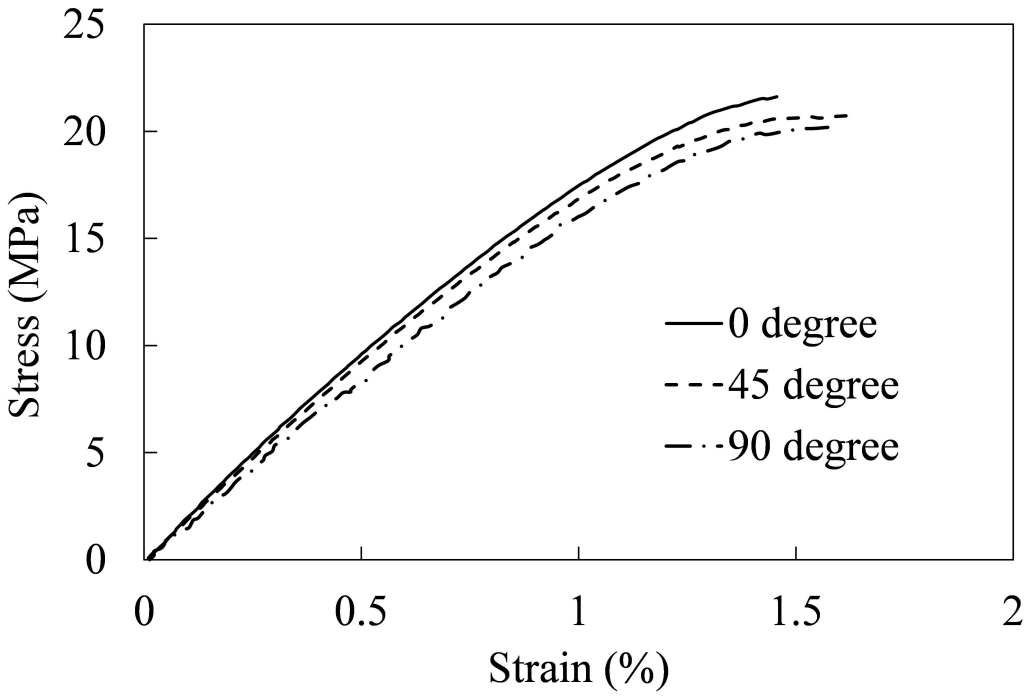

Fig. 2.16. Stress-Strain Curve of ABS Tensile Bars in Different Printing Orientations

The main reason why 0° has a relative large ultimate strength is the loading direction during the tensile test is aligned with how the sample being printed during the process. An article also shows that average the Youngs modulus of 3D printed ASTM D638 bar is 1.8 GPa, which is very close to our results [14]. This result indicates the best printing orientation is 0° when trying to achieve higher ultimate strength in applications. Reference has shown that the tensile strength of 3D printed specimen has nearly same strength, but inner structure has caused different time before fracture [15].

3. NUMERICAL METHOD ANALYSIS OF TENSILE TEST

3.1 Model Description

3.1.1 Model ASTM D638 ANSYS Tensile Analysis

Since the ASTM D638 a perfectly symmetrical structure, weight evenly on both sides of the specimen, therefore, apply force on one side of the specimen can reach the analysis of the overall sample. It can also help to reduce the step of a simplified analysis of ASTM D638. This numerical test can be done in three steps, first, the modeling of ASTM D638 in finite element analysis software ANSYS. Second, use finite element analysis software ANSYS to perform finite element analysis. Third, check specimen and structural optimization based on the results of finite element analysis model of specimen.

3.1.2 Specifics of ASTM D638

Taking into account the simplicity of the model structure, therefore it was not modeled in a 3D modeling software, but directly in the finite element analysis software ANSYS. This test is performed under finite element analysis software ANSYS, which developed to be large general purpose finite element analysis (FEA) software ANSYS. Model analysis, including setting job name and title, define the element types and material properties, 3D model and mesh, and define the load type and amount, and analysis structure. Due the nature of the ANSYS [16], the parts are assumed 100% fill, which results no gap inside of specimen.

3.1.3 Defined Cell Type

During finite element analysis, the analysis should be based on the geometry of the problem, the type of analysis and the analysis of the problem's precision requirements, and the type of unit selected for detailed analysis. This test selected four-node Shell element SHELL181. SHELL181 is suitable for analyzing thin to moderately-thick shell structures. It is a four-node element with six degrees of freedom at each node: translations in the x, y, and z directions, and rotations about the x, y, and z axes. The degenerate triangular option should only be used as filler elements in mesh generation. SHELL181 is well-suited for linear, large rotation, and large strain nonlinear applications. Change in shell thickness is accounted for in nonlinear analyses. In the element domain, both full and reduced integration schemes are supported. SHELL181 accounts for follower effects of distributed pressures [17].

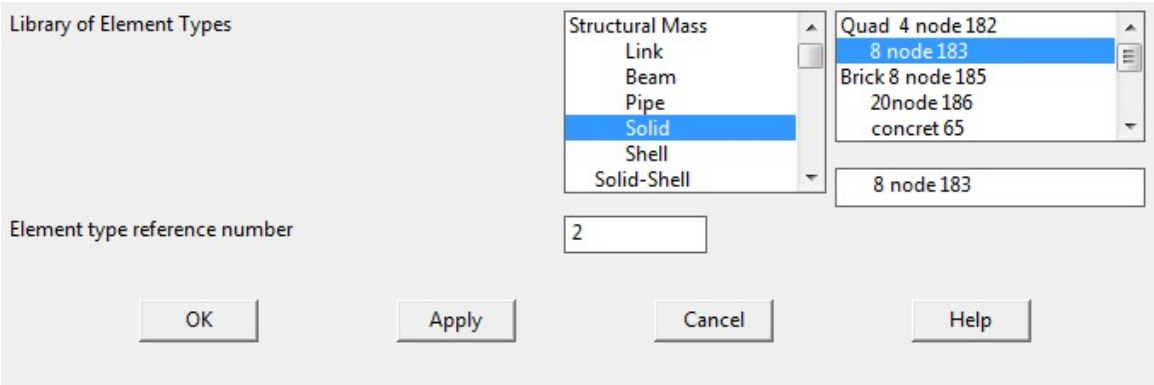

Fig. 3.1. ANSYS Set-up 8 Node 183

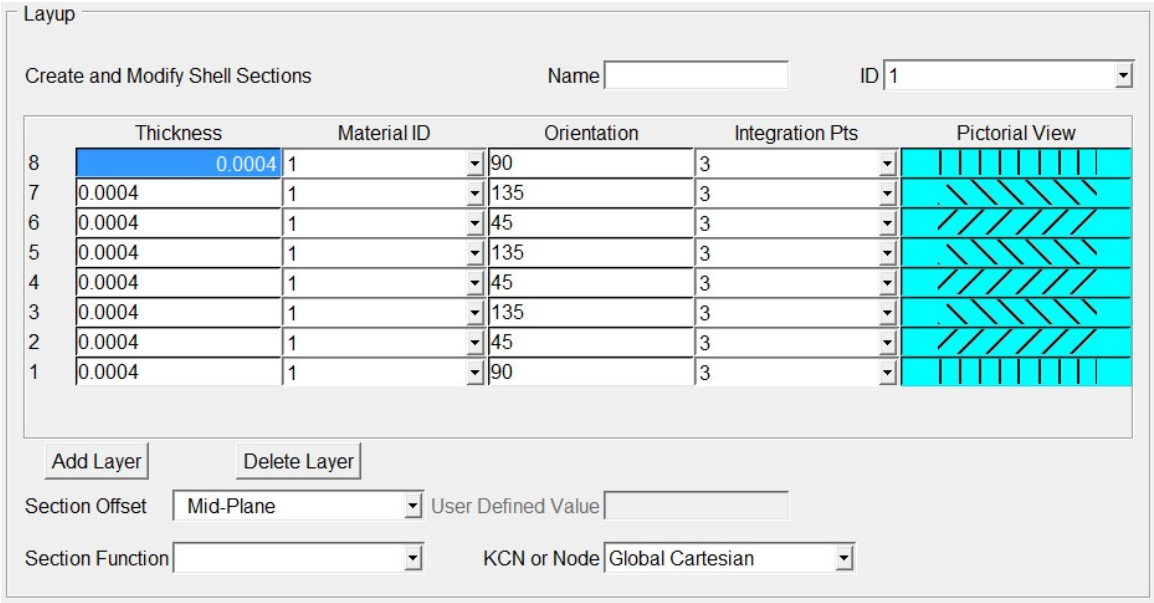

Fig. 3.2. ANSYS Set-up Layer Orientation

3.1.4 Define Material Properties

Due to the materials used for the ASTM D638 ABS plastic, it is possible to look up the elastic modulus of ABS plastic is 2.344 GPa in horizontal direction and 1.172 GPa in other directions, Poisson's ratio is 0.35 in horizontal direction and 0.175 in other directions, assume the material is non-compressive and format as laminates. From the main menu Preprocessor, Material Props, Material Models command, open the Properties window to define material models for elastic modulus and Poisson's ratio can be set. Reference [15] shows treating ABS 3D printed parts as composite material, however the layer bond in between would not reach perfect condition, but still assume the 3D printed part are bonded ideally in order to process to analysis.

	T1
Temperatures	0
EX	2.344E+009
EY	1.172E+009
EZ	1.172E+009
PRXY	0.35
PRYZ	0.175
PRXZ	0.175
GXY	8.96E+007
GYZ	8.96E+007
GXZ	8.96E+007

Fig. 3.3. ANSYS Set-up Materials Properties

3.1.5 3D Solid Model of ASTM D638

From the main menu click through Preprocessor, Modeling, Create, then Key points, In Active CS command to create four key points. Then select from the main menu Preprocessor, Modeling, Create, Areas, Arbitrary, Through KPs command, were picked up on four key steps in creating a generation of plane. Then from the main menu, select Preprocessor, Modeling, Operate, Extrude, Areas, Along Normal command, pick-up step to generate a surface to be stretched into one entity. Due to the length of the area only for the weight of the sample load range, so the sample load the stent surface to create three parts. Finally, from the main menu, select Preprocessor, Modeling, Operate, Booleans, Add, Volumes command, the 3D solid model of specimen created.

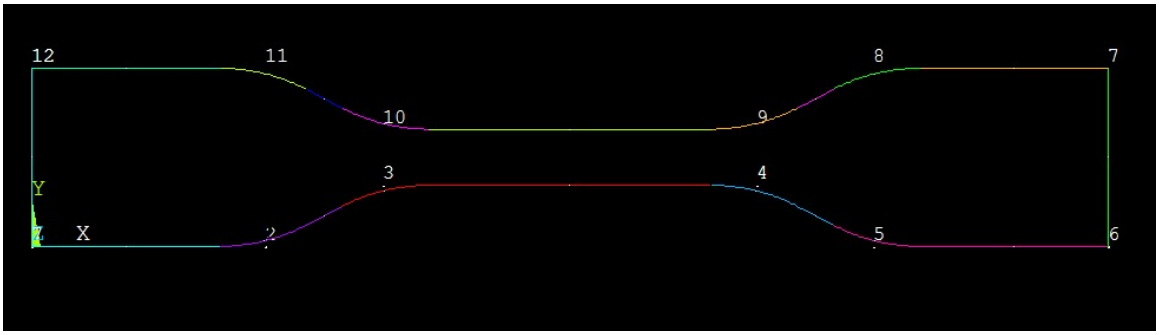

Fig. 3.4. ANSYS Model with Key Points

3.1.6 Solid Model Meshing

From the main menu, select Preprocessor, Meshing, Mesh Tool command, open the Mesh Tool (Grid Tool), check the Smart Size slider is set to the default value of 6, Mesh object selection Volumes, then click Mesh, entity selection dialog box opens, click Pick All button on the ASTM D638 model mesh, which is shown in Figure 3.5.

After model mesh finished, the next will be finite element analysis, which includes the definition of load and boundary conditions, and then solve the current model.

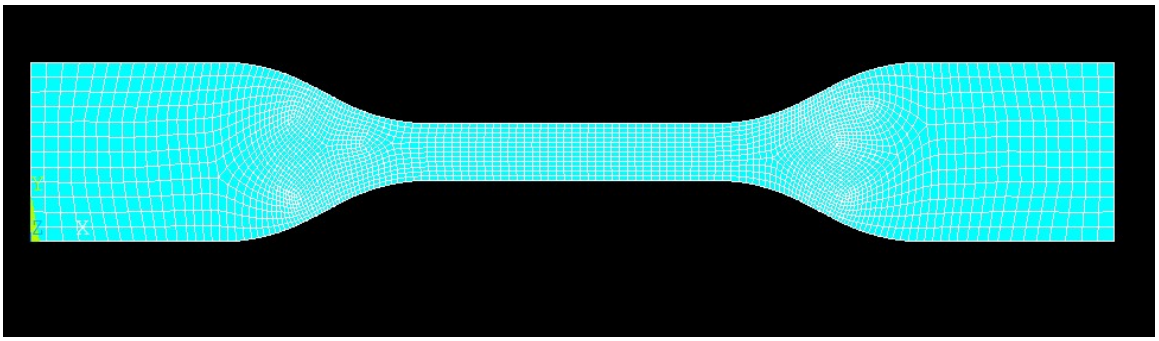

Fig. 3.5. ANSYS Model after Mesh (Front View)

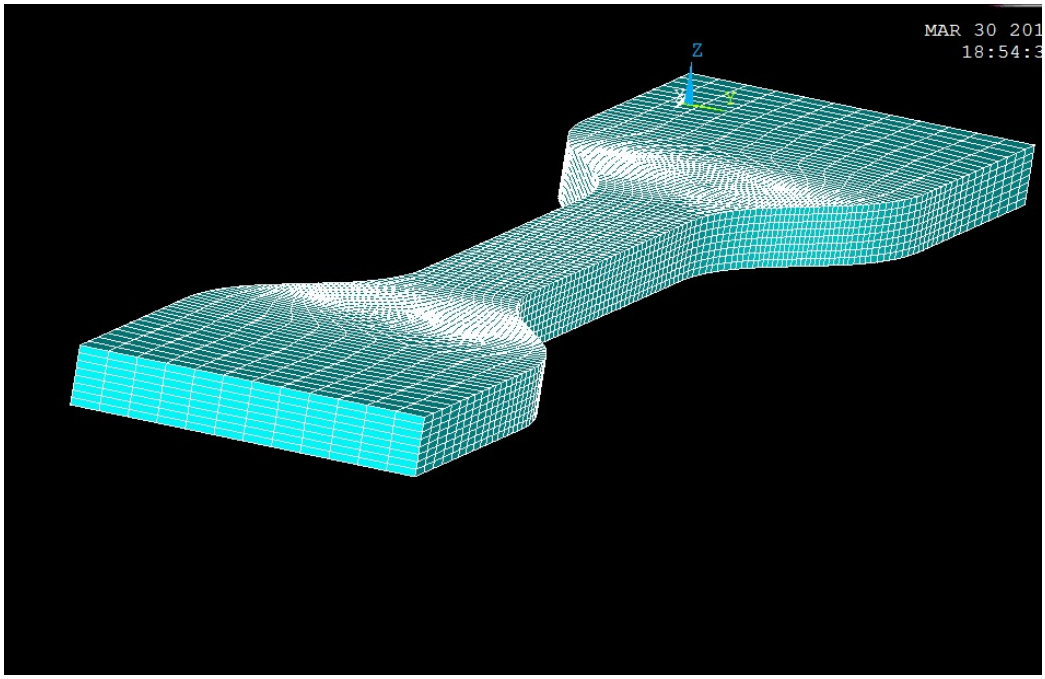

Fig. 3.6. ANSYS Model after Mesh (Side View)

After model mesh finished, the next will be finite element analysis, which includes the definition of load and boundary conditions, and then solve the current model.

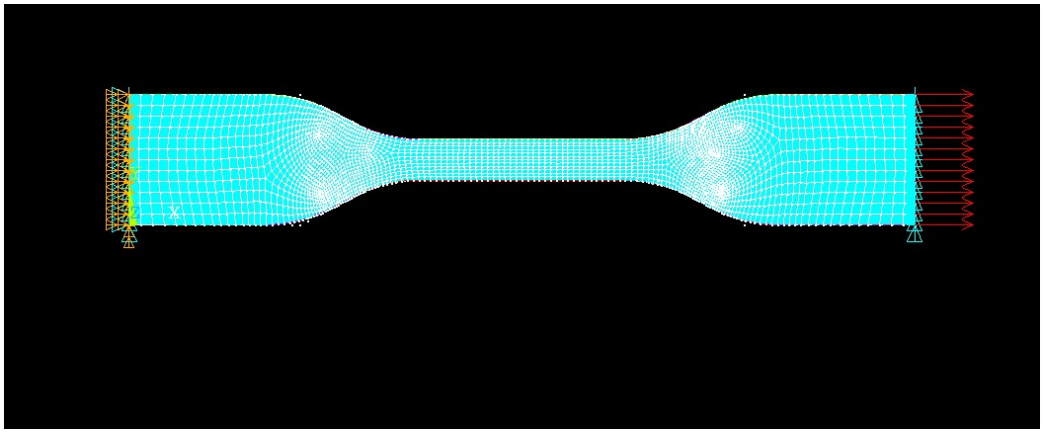

Fig. 3.7. ANSYS Applied Force and Fixture

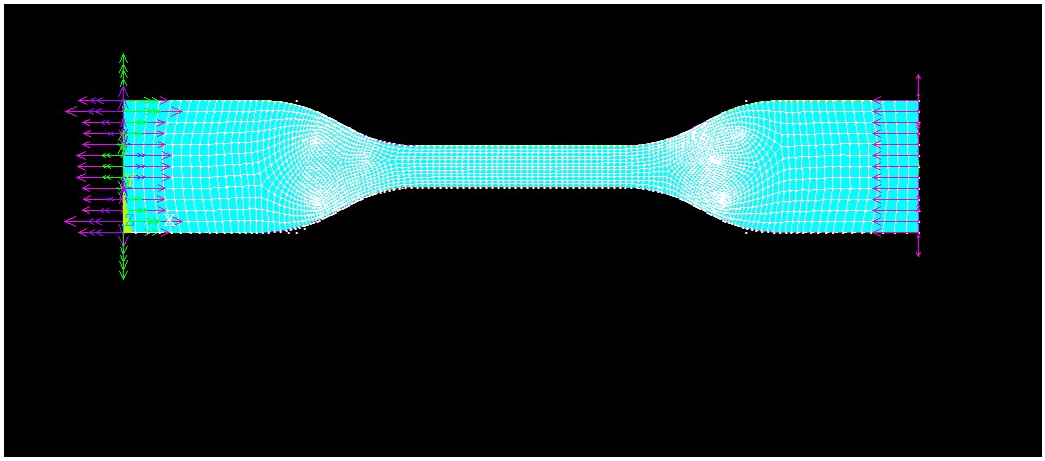

Fig. 3.8. ANSYS Reaction Force

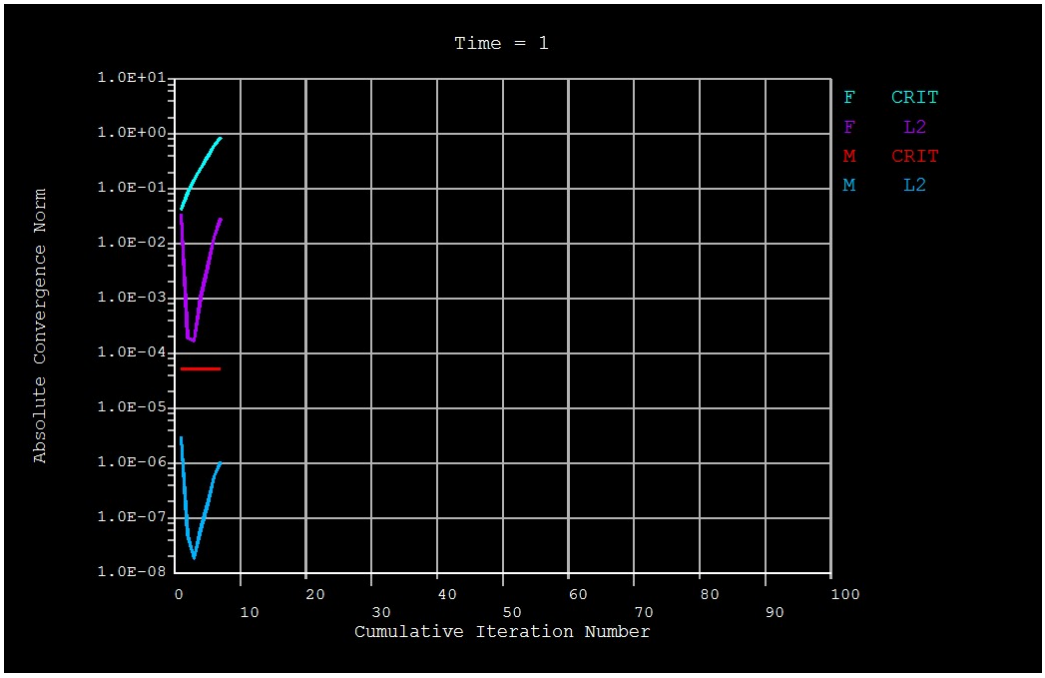

Fig. 3.9. Convergence Force on Different Point

3.1.7 Definition of Load and Boundary Conditions

Only one side of the specimen is going to apply force, other side of the sample to set as fixed in displacement and rotation. According to the characteristics of the real world test machine, in which the boundary conditions simplify the stand near the end surface of the side wall, the freedom of all to define loads and constraints will be fixed. From the ANSYS main menu, select Preprocessor, loads, Define loads, Apply, Structural, pressure, on Areas pick-up dialog box pops up, pick up the required loading surface, above the input force value is then calculated on the bracket close. The end face of the wall side constraints, select Preprocessor, Loads, Define Loads, Apply, Structural, Displacement, on Areas pick-up dialog box pops up, pick up close to the wall bracket in the face that the freedom of all constraints from the main menu. Then it is solved, select from the main menu Solution, solve, Current LS command, a confirmation dialog box opens and the state table for a list of the information in the confirmation, click [OK] button to start the solution. After the completion of solving, close the dialog box, click the [Close] button to close the dialog box prompts.

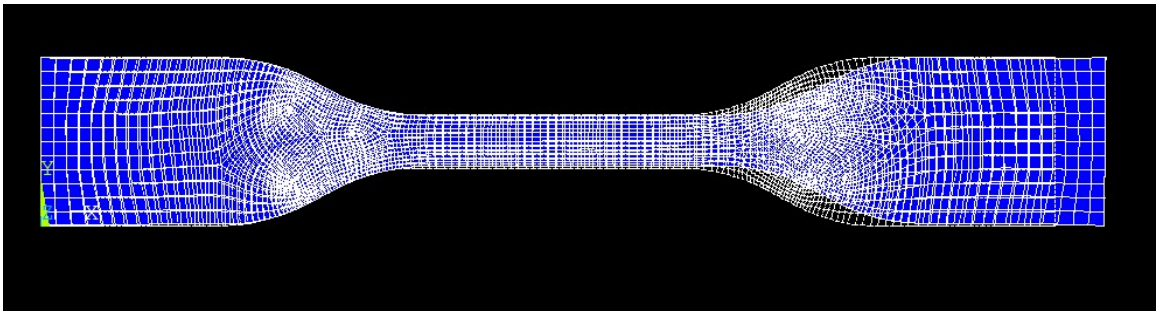

Fig. 3.10. Deformed Shape Compared with Original Model

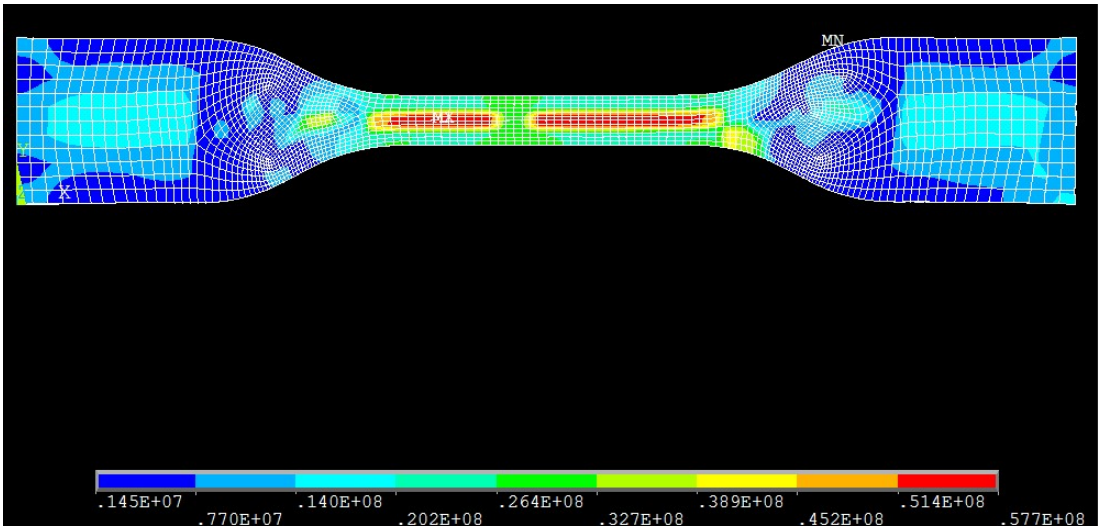

Fig. 3.11. ANSYS Stress Concentration (Front View)

3.2 Results and Discussion

3.2.1 ANSYS Graph

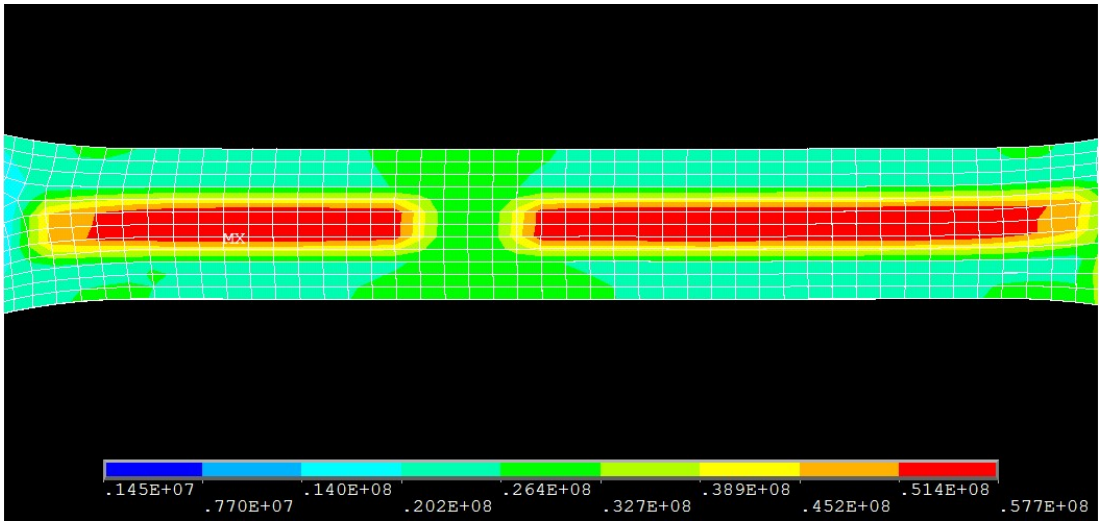

Fig. 3.12. Stress Concentration in the Middle Section (Top View Enlarged)

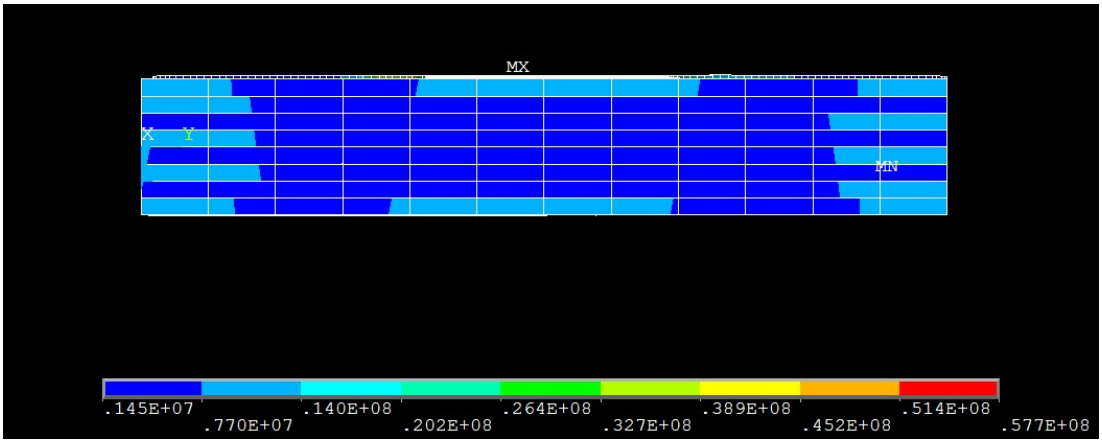

Fig. 3.13. Stress Concentration (Right Side View)

3.2.2 Strength Check

Due to the materials used for the ASTM D638 is ABS plastic, according to the investigation from MATWEB, obtaining tensile strength between 40 MPa to 60 MPa. From the finite element analysis results can be seen above the maximum stress in the X-axis is 57 MPa, which fall in the allowable stress. Therefore, the tensile test results meet the real world strength requirements.

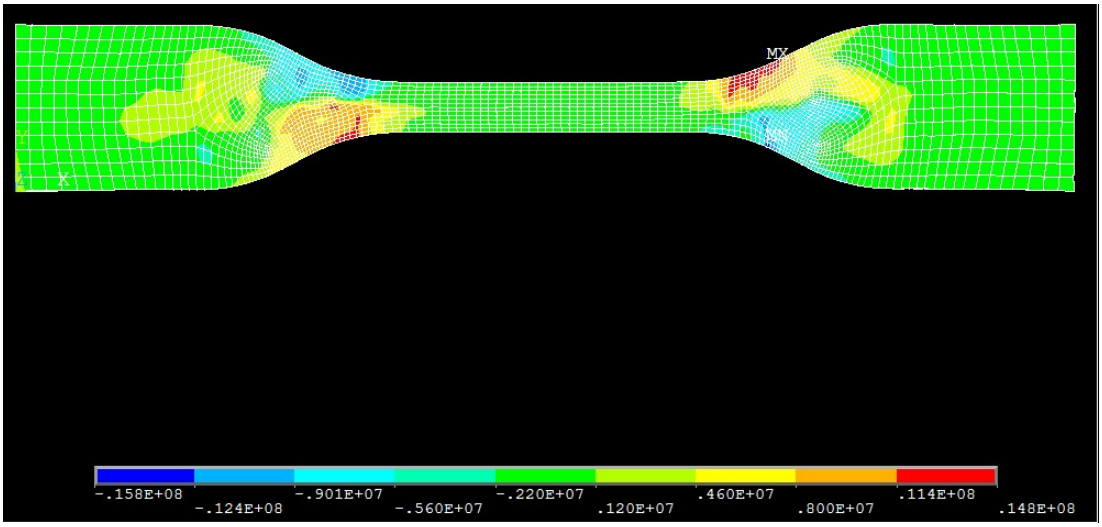

Fig. 3.14. Strain Concentration (Top View)

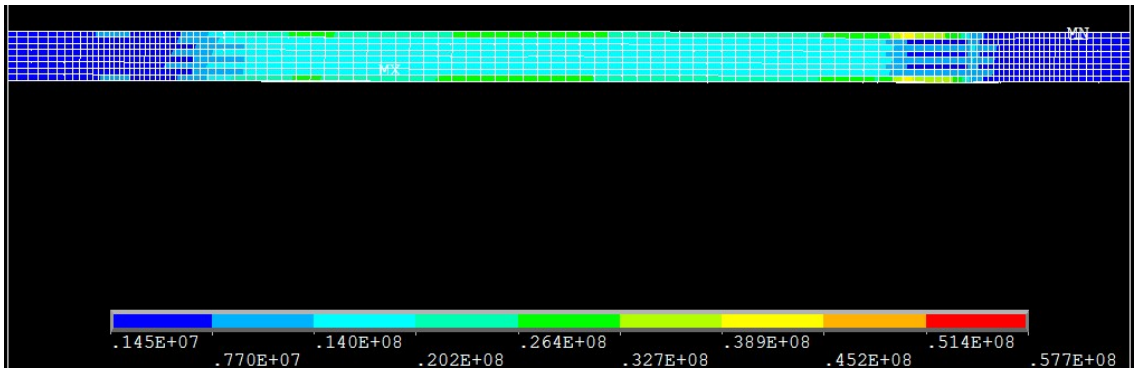

Fig. 3.15. Stress Concentration (Side view)

Compared with the end portion of the tensile specimen freely rotate, the presence of the end restraint specimens under normal circumstances, can result higher the peak value of the stress and strain. This indication can be observed in the ANSYS analysis, which Figure 3.10 is result after fix the right end from any rotation.

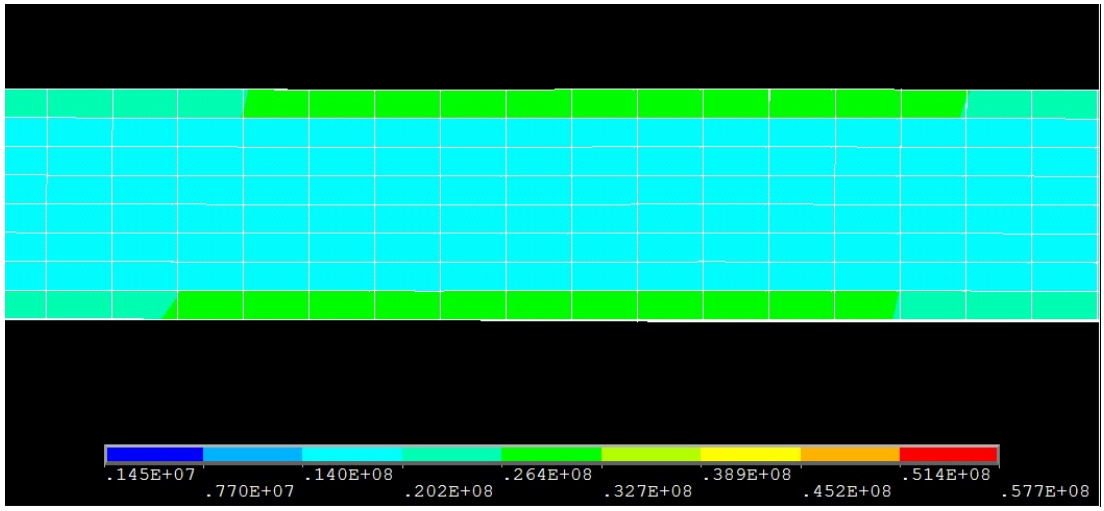

Fig. 3.16. Stress Concentration in the Middle (Bottom View Enlarged)

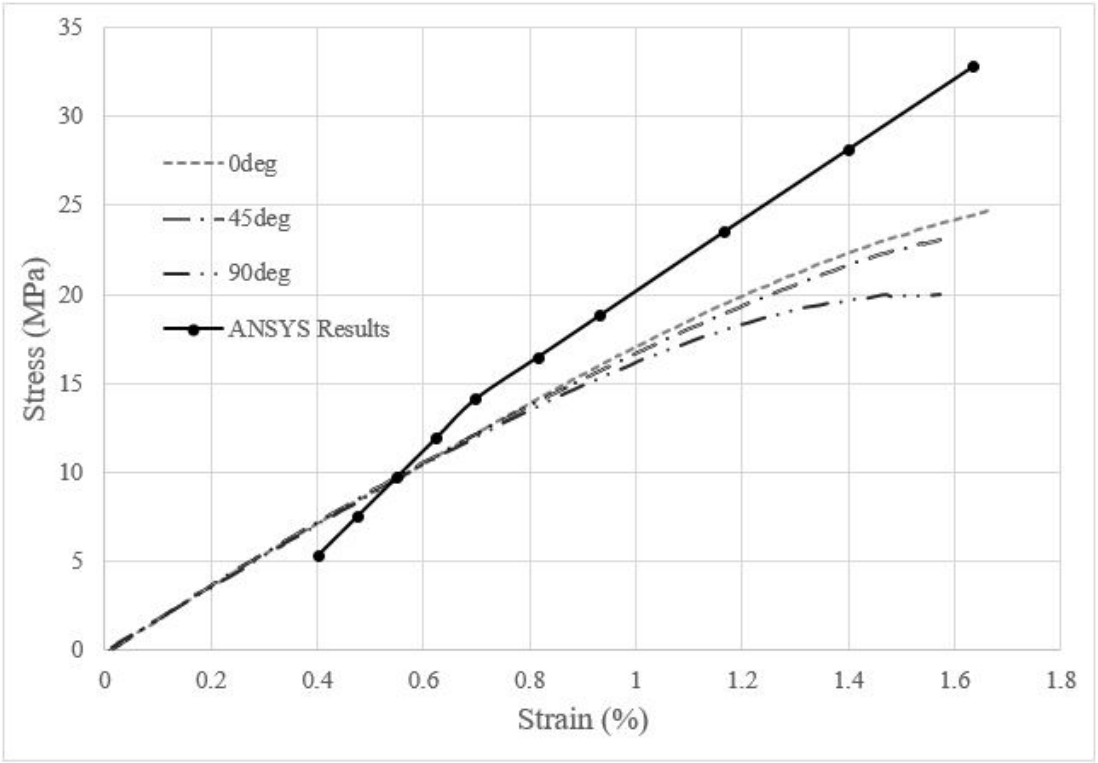

Fig. 3.17. Stress Strain Curve (ANSYS Results verses Test Results)

Based on the understanding and knowledge of the basic theoretical foundation finite element analysis and from the physical tests, found that ANSYS results can meet the real world material results. The tensile test results may have a downside which the correctness of the results calculated by finite element software still need to validate. In this research, only elastic analysis has been conducted; a plastic model study will show the tensile property under a large amount of load. In some cases, the computer calculated results are not necessarily correct, therefore after finished in the analysis, and the results need to compare with the theory calculation in order to make strong support of results data.

4. CREEP TEST

4.1 Experimental Detail

4.1.1 Materials

The specimens used in this study are designed in accordance with the ASTM standard test method for tensile properties of plastics. The printer used is a Dimension SST 3D printer in conjunction with CatalystEx software, both products of Stratasys Inc. The 3D printed specimen material used is ABS, also a product of Stratasys Inc. [18].

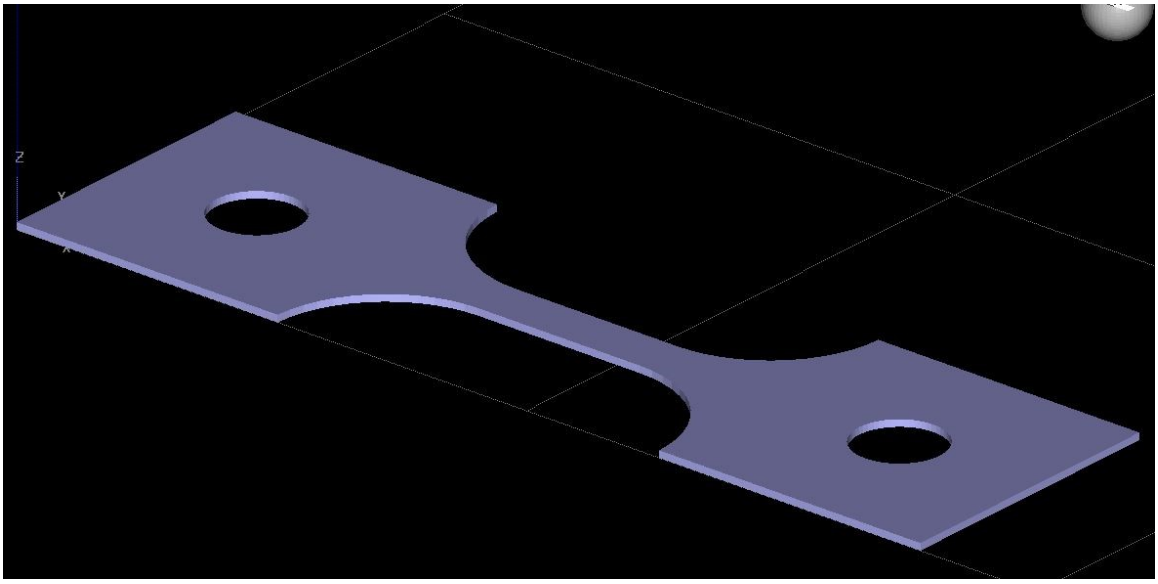

Fig. 4.1. 3D Model from Software

4.1.2 Printing Process

Fused deposition modeling is the 3D printing technique used to fabricate tensile test specimens. First, drawn a CAD model from a solid modeling software by using measured data of the physical model, then slice the CAD model with the data processing software which compiled into a bulk scan NC program. Figure 4.1 shows the completed CAD model in CatalystEX. Secondly, numerical control commands controls the motion of heated nozzle, which orderly deposit melted materials on a layer of sheet, including border outline and fill scan contours. After the completion of a stacked layer, printing platform descend one layer height, and then continue to deposit next layer.

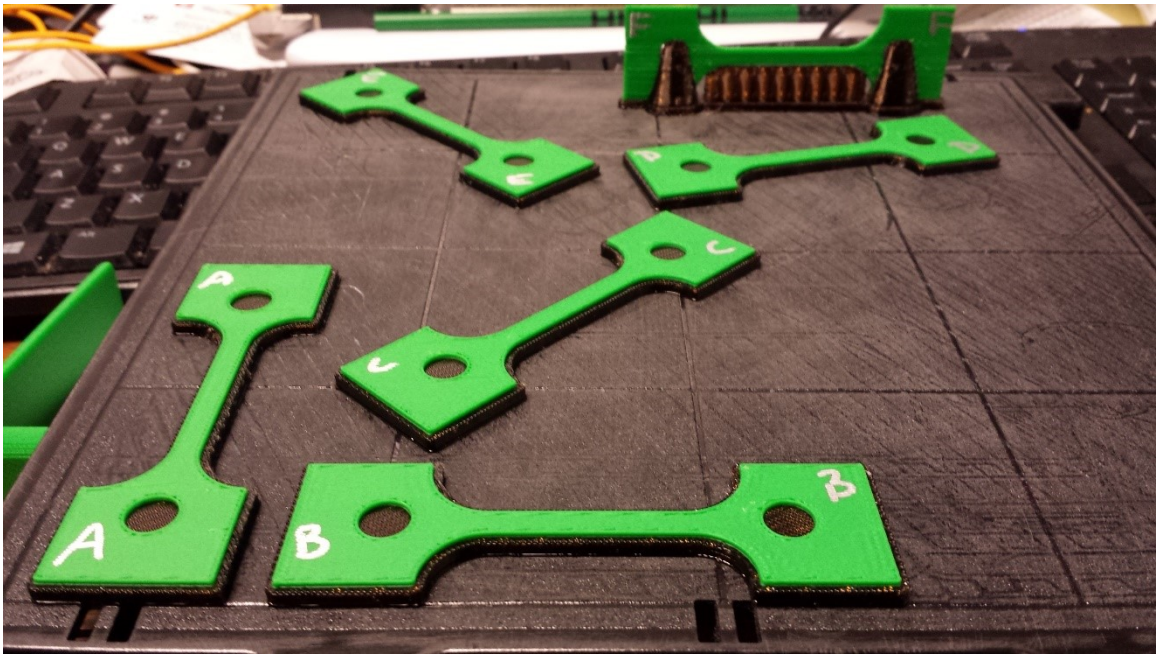

Fig. 4.2. 3D Printed Sample in Different Orientation

The printing process will finish till the completion of the accumulation of superimposed layers forming the whole entity. Print parameters through optimized as follows: melting temperature of 220 °C to 230 °C, the nozzle diameter of 0.5 mm, the print speed of 30 mm/s, layer height 0.1 mm, internal contour with 100% dense packing accumulation mode. During this creep test, three different angles (0 °, 45 °, 90 °) have been printed and tested. Figure 4.2 not only shows the 0 °, 45 °, 90 ° printing orientation samples which located at bottom left corner, but also shows extra samples were printed.

4.1.3 Test

Creep is a time-dependent deformation under a certain applied load. It is a challenging issue for applying time-dependent deformation with 3D printed internal structure, which is complex to assume linear elastic region during the first several seconds of loading [17]. This experiment is to perform a creep test on the 3D printed specimen. The main reason of this test is to observe the creep performance of 3D printed materials. Secondly, this experiment can show us the experimental curve of strain versus time under different printing orientation. In this case, the test environment is at normal room temperature. Figure 4.3 shows the creep measurement apparatus been used in creep test, which is model SM 106.

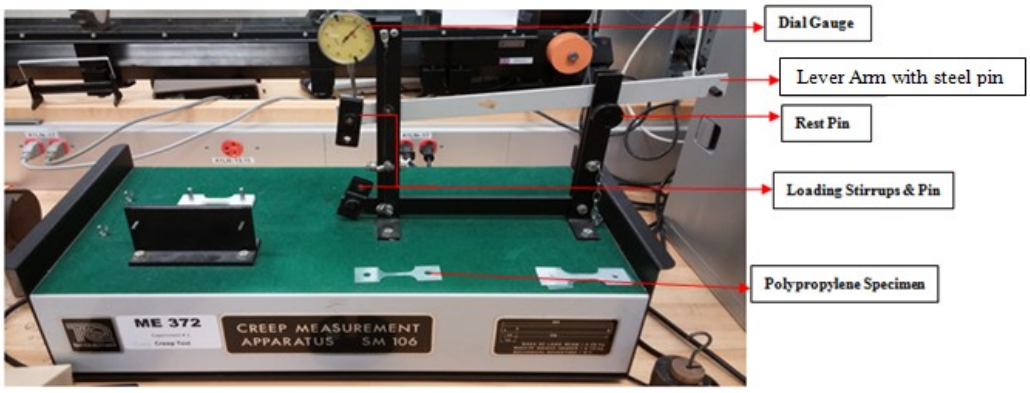

Fig. 4.3. SM10 Creep Apparatus (Front View)

In order to obtain the strain versus time creep curve, one 3D printed specimen has been applied with a small, but constant load. The 560 grams of weight were chosen to be the load number. Upon completing the experiment, it was evident a significant amount of deformation occurred within the initial 30 seconds the specimen was exposed to the load and after that the rate of deformation continued in a much slower, linear model of behavior. After 20 minutes, measure the maximum elongation, the load will take off from specimen allowing it to recover if it is not broken. Immediately the specimen shrank the length which is close to original length. We then measured the deformation in the specimen at equivalent time intervals.

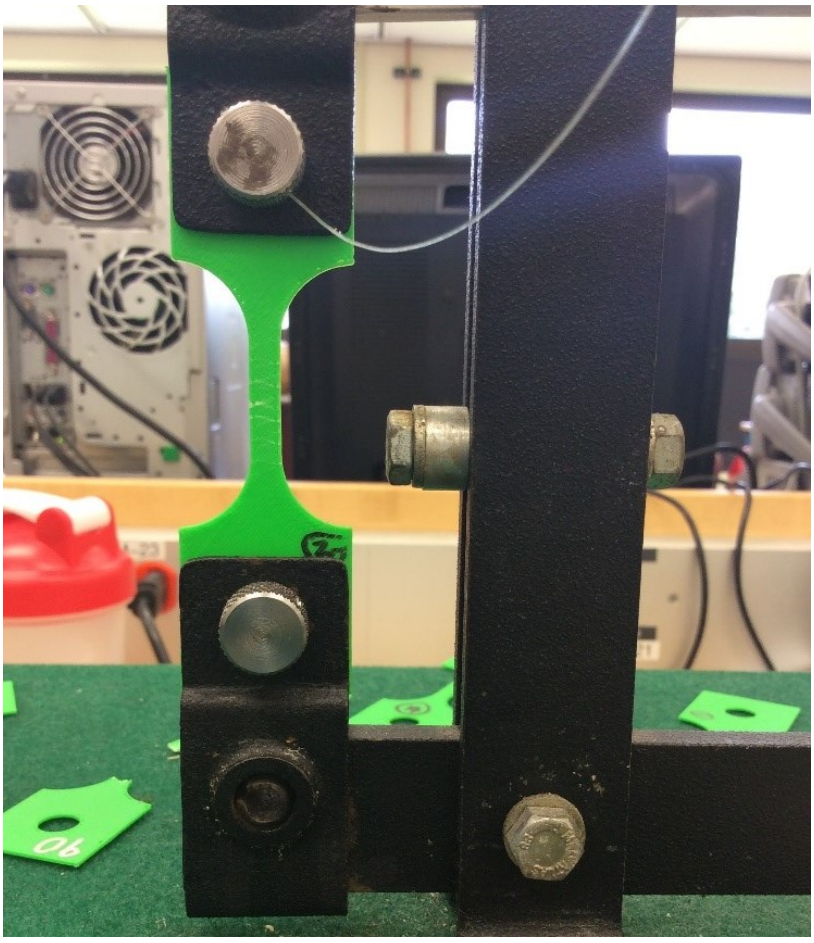

Fig. 4.4. SM10 Creep Apparatus with 3D Printed Specimen

From this experiment, we were able to obtain a creep curve and a creep constant for 3 different angles of printing orientation material. However, both 0° and 45° did not complete the entire test before the break. Figure 4.4 shows one of the specimen has been loaded on the apparatus, some crack start to show after pulling the reset pin.

4.2 Results And Discussion

4.2.1 Data

Table 4.1
Sample Data Measured Creep from 3 Different Print Orientation at Time Interval

	0 Degree Average	45 Degree Average	90 Degree Average
	Weight(G)	Weight(G)	Weight(G)
	560g	560g	560g
Time	Elongation	Elongation	Elongation
(Second)	(0.1mm)	(0.1mm)	(0.1mm)
0	5	5.05	4.85
30	5.35	5.5	4.95
60	5.6	5.7	5
90	5.8	5.85	5
120	5.95	5.9	5
150	6.2	6	5.1
180	6.4	6.05	5.1
210	6.7	6.1	5.2
240	7	6.2	5.2
270	7.5	6.4	5.25
300	7.8	6.55	5.25
330	8.1	6.65	5.3
360	8.5	6.75	5.4
390	9	6.8	5.45
420	9.3	6.9	5.5
450	10	7	5.5
480	11	7	5.55

Table 4.1 shows partial data of entire data pool we collected. After gathering data from each printing orientation, the average number of elongation has been calculated. The early breakers (specimen break before first 150 seconds) are being considered as outliers. Most of the possible errors in this experiment would result from the possibility of slippage in the test apparatus. If at any point there was a lessened strain, because the apparatus could not hold the test material in position, then the values were compromised slightly, as the actual strain was less than the assumed strain, giving a bit of inaccuracy. Also, there was the possibility of human error in getting precise readouts at the exact time needed for a flawless experiment, as each of the readings were taken at intervals of thirty seconds over the course of twenty minutes total. This made it difficult to get the right readings at the exact times, without rounding. Finally, there was the presence of instrument error, as the instrument used to measure the amount of creep only had marked measurements to the nearest tenth in units of 0.1 mm.

4.2.2 Load and Elongation Curve

Figure 4.5, below, is a plot of the elongation of the material versus time, as the weight force of 560 grams was being applied for the first eighteen minutes. Then, as the weight was removed at the fifteen minute mark, the graph shows a sharp drop, where the material quickly relaxed without under the decreased load and strain. However, the 0° and 45° printing orientation was not able to endure the load and broke before 500 seconds and 780 seconds respectively.

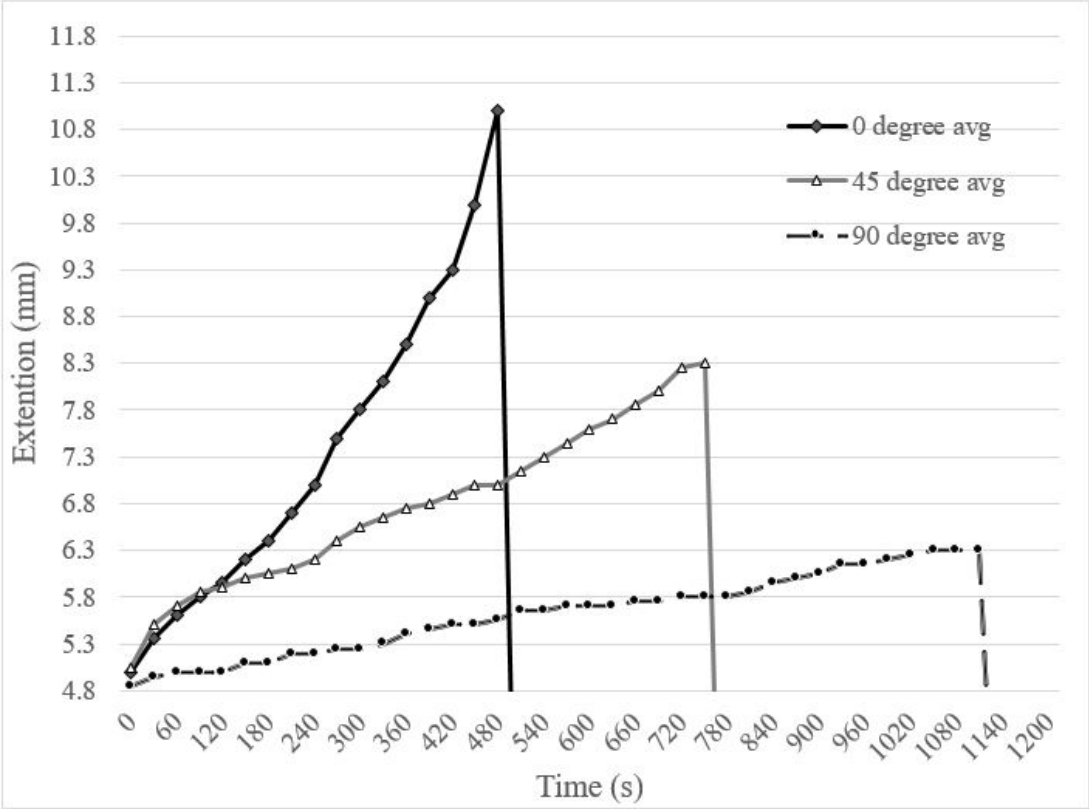

Fig. 4.5. Plot of Elongation of Test Material versus Time

The creep curve was not able to be observed for ABS materials during the creep recovery. In Figure 4.5 shows where the primary creep is because the elongation starts to diminish due to work hardening of the material, but for plastics this process cannot be determined due to work hardening. Polymers consist of chain-like molecules that are tangled. The creep occurs when chains untangling and slipping. However the 3D printed specimen created by a string of melted ABS material, therefore, its composite-like structure does not provide as many tangled chains as normal polymers. Once we released the weight of the specimen, the graph shows how 90° printing orientation recovered from the elastic deformation. Once it recovered almost completely it then started to taper off where the creep recovery region is found.

The following equation is the most commonly used in analyze plastic creep model of empirical equation [19]:

$$\varepsilon = \varepsilon_0 + B\sigma^m t^k, \text{ where } B = \frac{A_2}{d^q T} \exp \frac{-Q}{RT}$$

Where ε is the tensile creep strain, t is time , σ is the applied creep stress, ε_0 is the instantaneous loading, $A2$ is activation energy, q is average grain diameter, T is temperature, and B, m, k are constants for a given materials [19]. A plot of $log\varepsilon$ against $logt$ will therefore be linear and the slope will give the value of exponent k. In this research case, we have calculated three different k value because of the variation of printing orientation. After obtaining data with different orientation, the B, m, and k value of 0° printing orientation was calculated.

Table 4.2
k Value verses Printing Orientation

Printing Orientation	0°	45°	90°
k	0.455	0.243	0.200

Table 4.3
B, m, k Value at 0° Printing Orientation

Printing Orientation	B	m	k
0°	0.000126	0.321	0.455

The ABS specimen studied had a relatively linear increase of elongation while the load was on, however, was able to recover significantly when the tensile load on the creep apparatus was taken off. This has partials caused with the elastic properties of ABS material and their ability to physically resemble Hooks Law closely. ABS materials are considered to be in the primary creep stage. The strain decreases as the printing orientation increased from 0° to 90°.

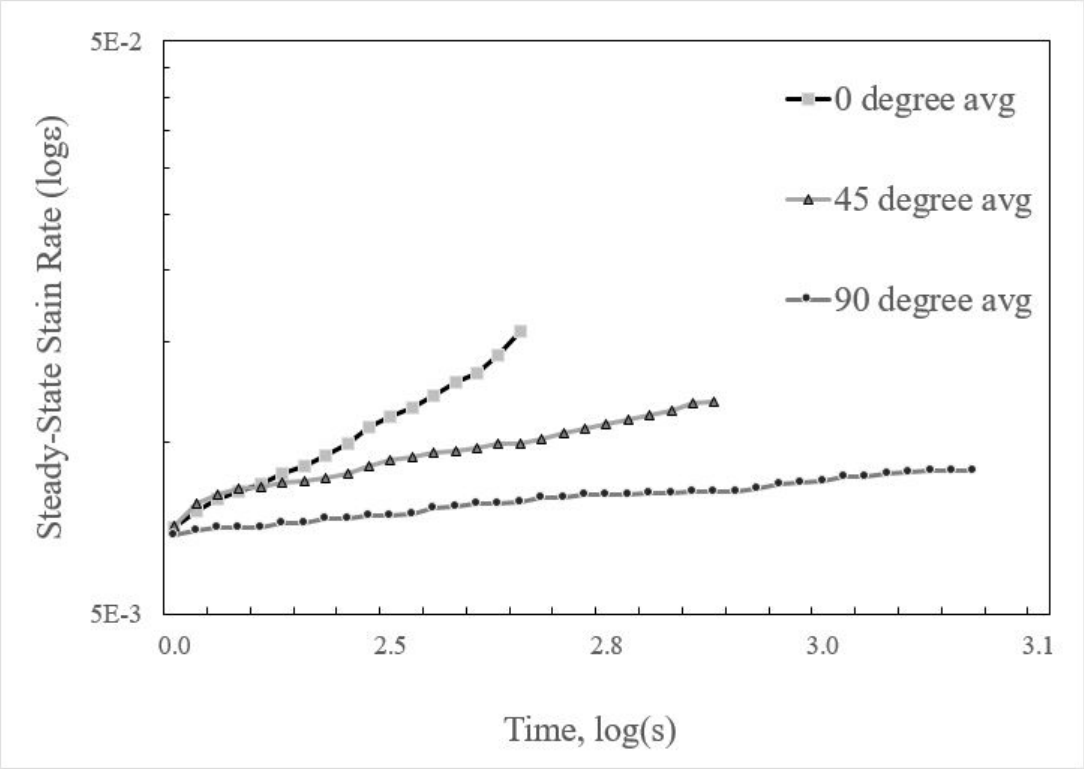

Fig. 4.6. Steady-State Strain in Log Scale versus Time in Log Scale

If further creep experiment will be done in the future regarding 3D printed model, the layer number of specimens and the weight of the load should be varied. This will give even a better understanding of the ABS material and how it will respond to varying levels of mechanical stress relative to the specimens layer or printing orientation. Ways to improve the study also may include repeating the experiment more times to derive to more accurate conclusions along with recording the elongation of the specimen in smaller increments to get a more accurate model comparing elongation versus time.

5. FATIGUE TEST

5.1 Experimental Detail

5.1.1 Materials

The specimens used in this study are designed in accordance with the Terco material test method for fatigue properties. During the test, materials will undergo many levels of stress. A measurement of this property can be obtained by means of fatigue test. The common stresses or loads are tensile, compression, bending and rotary bending. The printer used is a Dimension SST 3D printer in conjunction with CatalystEx software, both products of Stratasys Inc. The 3D printed specimen material used is ABS, also a product of Stratasys Inc.

Fatigue properties of 3D printed model can help people to understand the stress concentration and strain behavior in the specimen, which can provide a more reliable basis for estimating the fatigue life of the 3D printed model. Under fatigue loading, the material structures undergo an irreversible process of energy consumption, resulting in declining strength properties and dislocation, slip within the material and other defects, and ultimately lead to failure of the material. Fatigue damage plastic parts is the most common failure mode. It can be said fatigue strength are a measure of an important indicator of the durability of plastic, therefore, the fatigue life of 3D printed parts research and forecasting has great significance.

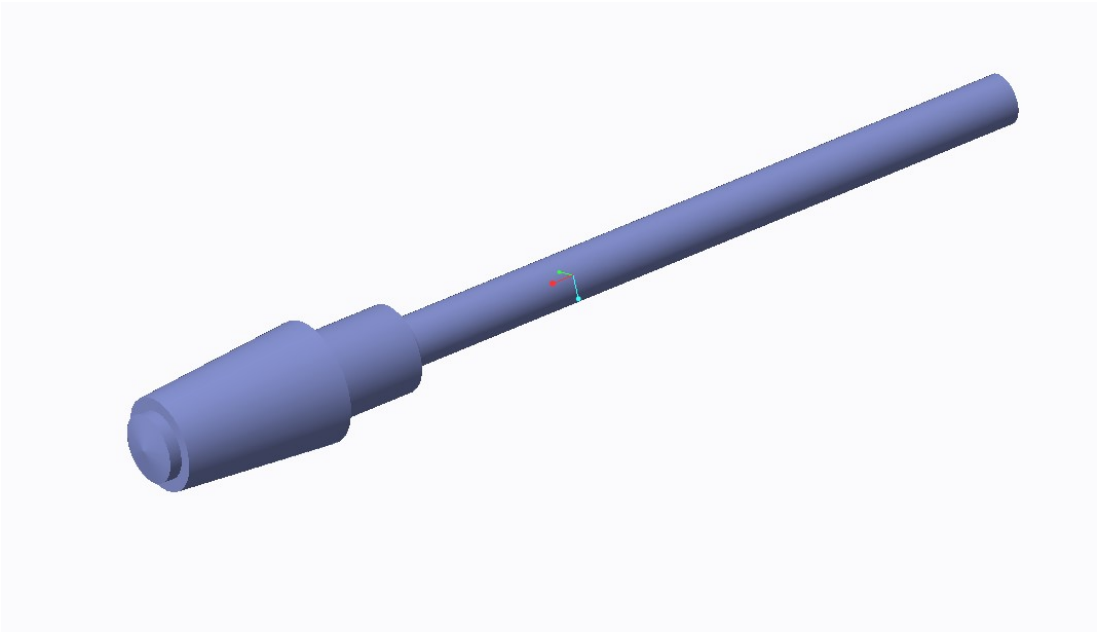

Fig. 5.1. 3D Model Showed in CREO

5.1.2 Printing Process

Fused deposition modeling is the 3D printing technique used to fabricate fatigue test specimens. First, drawn a CAD model (Figure 5.1) from a solid modeling software by using measured data of the physical model, then slice the CAD model with the data processing software which compiled into a bulk scan NC program. Figure 5.1 show the completed CAD model in CERO. Secondly, numerical control commands controls the motion of heated nozzle, which orderly deposit melted materials on a layer of sheet, including border outline and fill scan contours. After the completion of a stacked layer, printing platform descend one layer height, and then continue to deposit next layer.

The printing process will finish till the completion of the accumulation of superimposed layers forming the whole entity. Print parameters through optimized as follows: melting temperature of 220 °C to 230 °C, the nozzle diameter of 0.5 mm, the print speed of 30 mm/s, layer height 0.1 mm, internal contour with 100% dense packing accumulation mode. During this fatigue test, all the samples were printed in the normal position which is parallel to the bed shown as Figure 5.2. Because of its unique shape and size, the vertical print cannot be achieved.

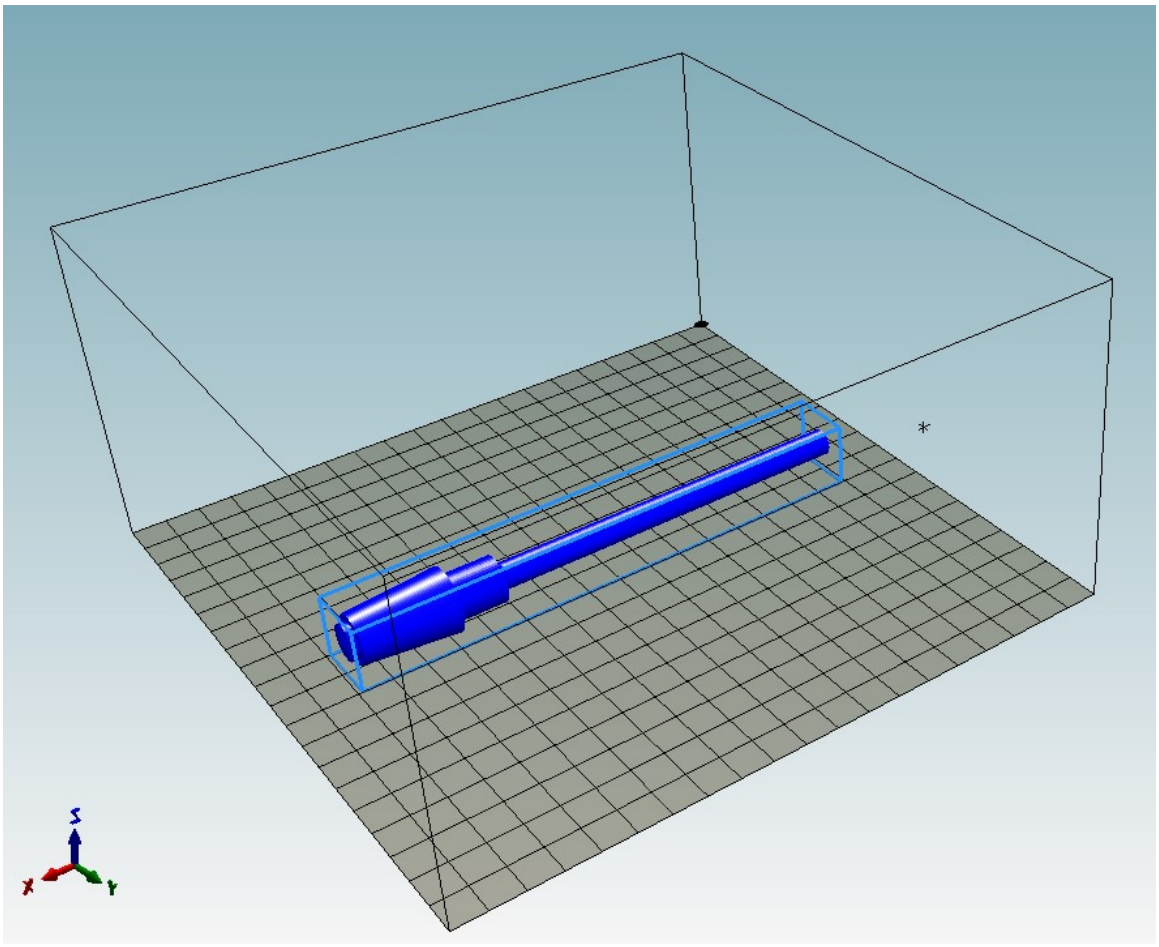

Fig. 5.2. Fatigue Model Showed in Slicing Software

5.1.3 Test

Fatigue property is an important material characteristic where fatigue fracture can caused by different type stress variations at a point even though the maximum stress is less than the proof or yield stress [20]. The static fracture is started by tensile stress with 3D printed gap or crack. Once started the edge of the crack acts as a stress stimulate and thus assists in the propagation of the crack until the reduced section can no longer carry the imposed load [21]. While it appears that fatigue failure may occur in all materials, there are marked differences in the incidence of fatigue [21]. To introduce this very complex subjects in a simple way, the apparatus demonstrates the classical fatigue experiments carried out by Terco. The fatigue test conducted by the machine made by Terco, model number MT 3012-E. It uses the method of reversing the stress on a part by employing a cantilever rotated about its longitudinal axis. Hence the stress at any point on the surface of the cantilever varied sinusoidal. This kind of test machine is the most commonly used in fatigue test, developed for analog shaft working conditions.

Fig. 5.3. Preparing the Test Piece

Figure 5.3 shows a rotating bending fatigue test machine, where the testing sample fasten from the left to right form into a whole as a rotating beam. The narrower side supported by rolling bearing, the wider side is connected to the motor, which is linked to counter that can record 7 figure numbers. The motor drive the specimen to rotate at a speed of 3000 revolutions per minute, power supply provided is 200V single phase. Attached to the shaft at the other end is a fixture. The loading device consists of a spherical ball bearing and a micro switch. By turning the loading wheel clockwise the loading on the test piece can be increased. A spring balance measures the loading value. The fatigue tester, which is designed to be placed on a bench, is very stable at 8 feet, weighing 24kg. The hanging weight does not move, but the sample is rotated, the specimen is subjected to symmetric cyclic bending stress. When the sample fatigue fracture, triggers the machine stop, then write down the cycle number N. The Figure 5.4 shows test data, N indicates elapsed revolutions since the RESET-button was pressed or the first start of the machine. F indicates the actual force applied to the test piece. LIM indicates the force-level where the test will stop. ORG indicates and save the value of the applied force when the test starts.

Fig. 5.4. The LCD-Display Showing Test Data

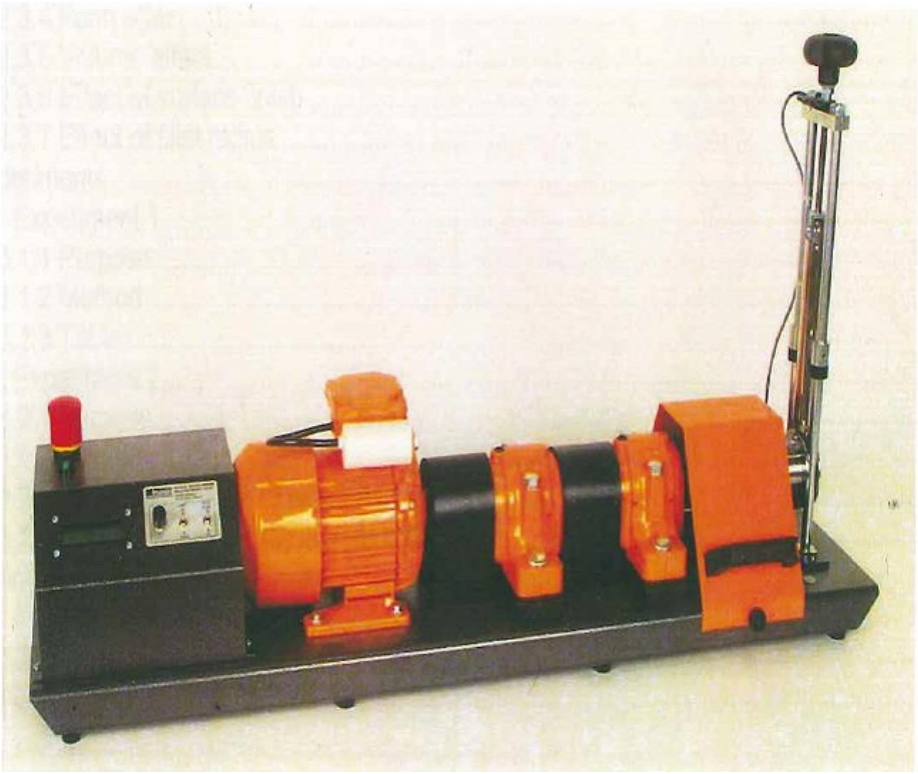

Fig. 5.5. The MT3012-E Fatigue Tester

5.2 Results and Discussion

5.2.1 Data

The cycle number of material experienced under alternating load before failure called fatigue life N. Applied stress is smaller, longer fatigue life. Any cyclic fatigue limit is higher than the maximum stress max, below a certain life cycle will correspond to base N. The maximum number of different cyclic stress tests obtained by fatigue life data as well as fatigue limit data to max vertical axis N as the horizontal, we can draw the maximum stress curve verses fatigue life, namely $\sigma_{max} - N$ curve, commonly referred to as $S - N$ curve. $S - N$ curve with stress to characterize the fatigue properties of the material. Figure 5.17 shows the general form $S - N$ curve of 3D printed ABS model with 90 ° printing angle.

Fig. 5.6. Fatigue Test with 30 N Load

Fig. 5.7. Fatigue Test with 30 N Load

Fig. 5.8. Fatigue Test with 40 N Load

Fig. 5.9. Fatigue Test with 40 N Load

Fig. 5.10. Fatigue Test with 50 N Load

Fig. 5.11. Fatigue Test with 50 N Load

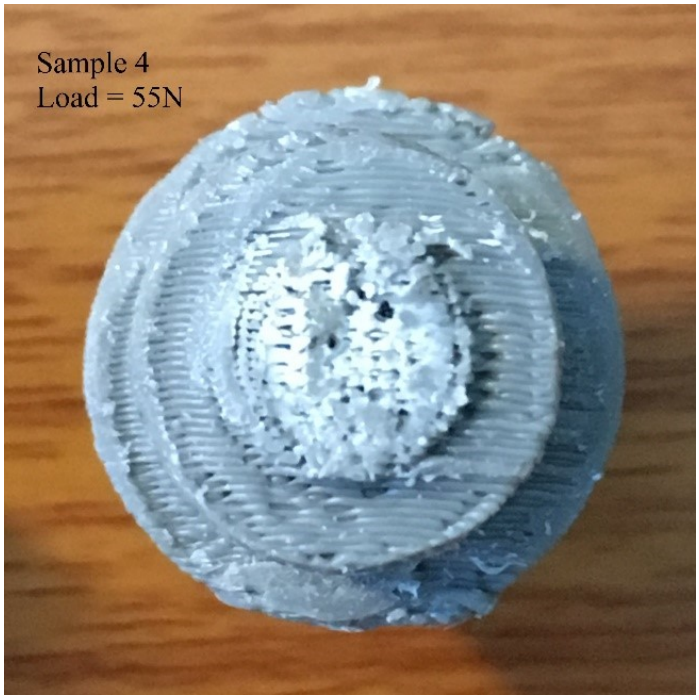

Fig. 5.12. Fatigue Test with 55 N Load

Fig. 5.13. Fatigue Test with 55 N Load

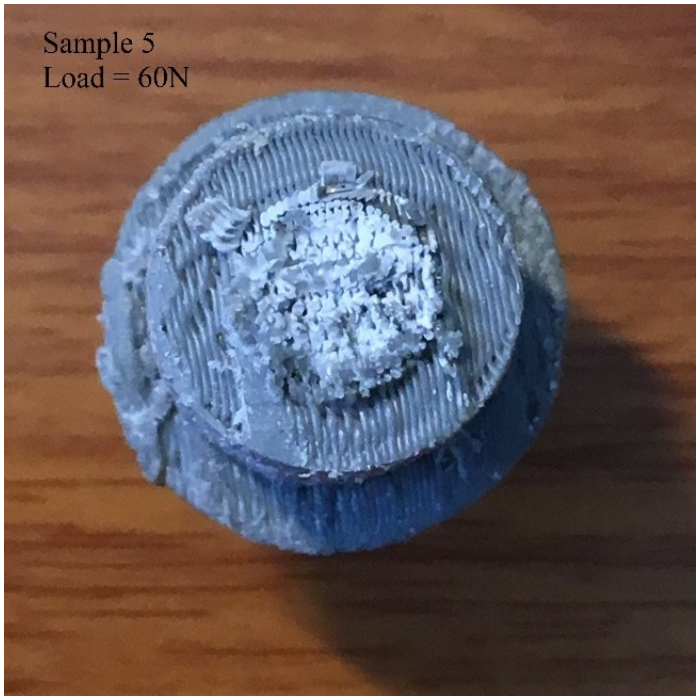

Fig. 5.14. Fatigue Test with 60 N Load

Fig. 5.15. Fatigue Test with 60 N Load

From all the samples above, a break occurred in the parts, and it is the result of stress under the rupture limit. Those samples have therefore been subjected to dynamic loading. Sample 1 (Figure 5.6) can clearly see both static fracture and fatigue fracture. Static fracture is based on one load which occurred in relatively white color part of the center of the sample. Outside of the center white part is called a fatigue fracture, which appears to be uneven surface compares to static fracture. Compressive tension and rotary bending are the causes of the fatigue fracture. As can be seen from the tension diagram, point A is the most susceptible and it is at this point that fatigue fracture was occurring during the sample test. The test piece broke at the radius of the fillet is due to the fact that the fatigue limit is not as constant for the material, but is dependent on other factors such as type of load, volume of material, surface finish and form [22]. At high stresses levels, short fatigue lives noticed accompanied by plastic strains.

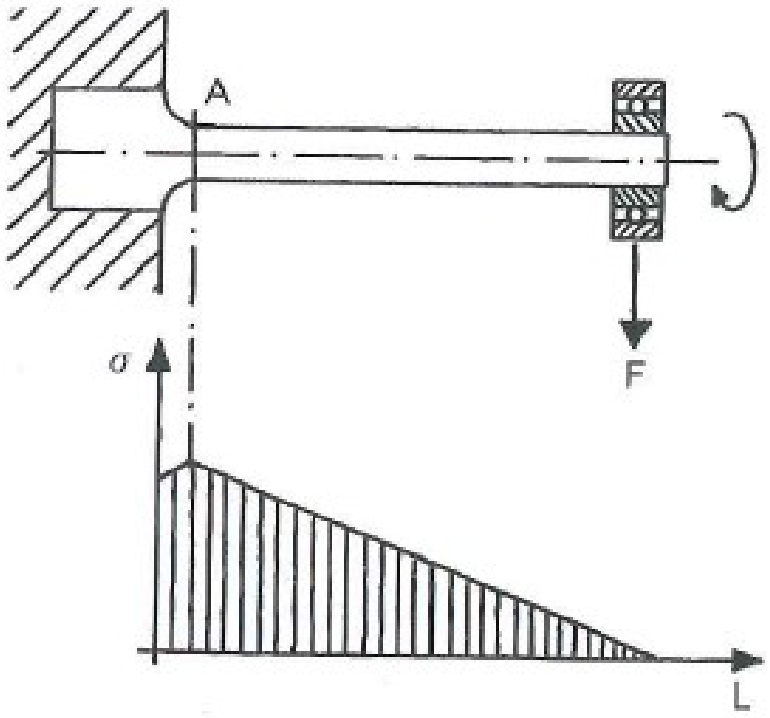

Fig. 5.16. Tension Diagram

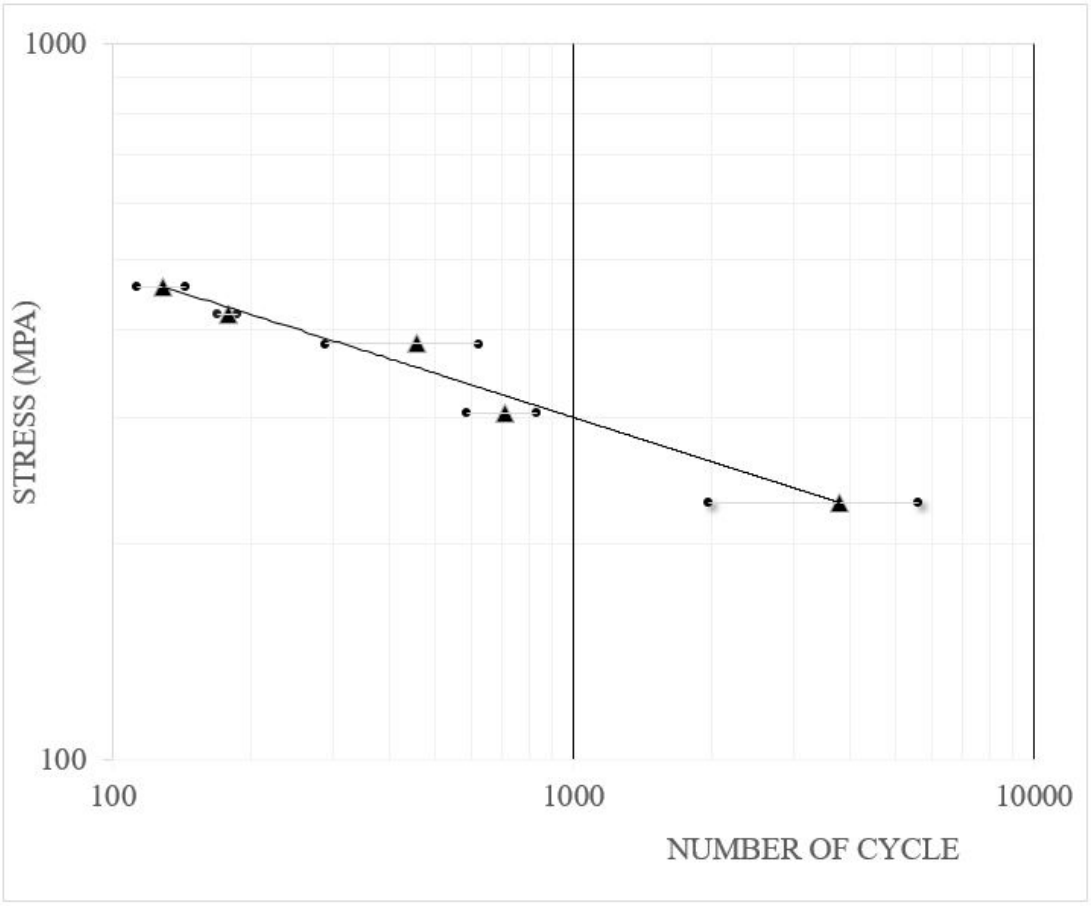

Fig. 5.17. $S - N$ Curve in Log Scale

To find the linear least-squares fit equation, obtain $log\sigma$ and $logN_f$, then perform least-squares fit to obtain A and B value of the $S - N$ curve. Since the machine runs at 3000 RPM, which is relatively fast rotation speed, however the samples were not showing any thermal melting effect because of the short amount of run time. Therefore, the following calculation was based on no heating assumption. The cycle number of failures increases dramatically, with stress level decreases and may change over into different magnitude. Therefore, logarithmic scale is used in x-axis. Since single log plot cannot be read accurately, logarithmic scale is also used in the y-axis.

During the test, stress levels at all levels should be carefully selected so that a small number of samples measured with desirable results. The Table 5.1 shows the values of A and B from the rough solutions and refined solutions are relatively agreeing with each other in general. Since the cycle number is below 10^5, the fatigue model can refer as low-cycle fatigue.

5.2.2 Discussion

Many engineering components are stress concentration area, such as holes, grooves, at the cross section of the transition, the internal defects. When the specimen experiencing cyclical external loads, although it is still at elastic range of work, but in the material stress concentration area will enter the inelastic state. With the increase of external load of cycles, cyclic stress concentration of plastic strain resulted in crack initiation, expands to make specimen fracture. For data approximating a straight line on a log-log plot, the corresponding equation [19] is

$$\sigma_a = AN_f^B$$

Both A and B are fitting constants, A has unit of MPa, B is dimensionless.

Table 5.1
Fitting Constants A and B

Constant	**A (MPa)**	45 °
Test Average	1283.338	-0.198
Fit Equation	1336.634	-0.205

The crack is shown on Figure 5.14 can dramatically reduce the life of this fatigue bar. By applying Paris Law, fatigue crack growth can be calculated with following equation:

$$\frac{da}{dN} = C(\Delta K)^n$$

Where K is stress intensity factor, C is material constant, N is cycle number, and da/dN is m/cycle [23].

With the crack size of the 0.75 mm long, then apply the Paris Law equation. Found that the stress intensity factor is varies from 352 to $700MN - m^{\frac{3}{2}}$, therefore, the fatigue crack growth rate is 0.0341 mm/cycle. However, if the crack size is 0.6 mm long, then the stress intensity factor will vary from 315 to $630MN - m^{\frac{3}{2}}$, resulting the fatigue crack growth rate become 0.0269 mm/cycle. Despite the increasing cycle number with large amount of load, surprisingly small differences in the crack length can have a large effect on the crack growth rate. Therefore, when choosing the printing parameter, 100% infill would results, lower fatigue crack growth rates.

As a consequence of the 3D printed model which shows on $S-N$ curve figure, the model can be used in aircraft interior or other similar applications. However, when designing for infinite life (millions of cycles), such result may not exist and will take too long to reproduce. When the material to enter the plastic strain-based plasticity state, only a strain for the control parameters can be measured to take the fatigue properties of the material. Application of these materials provides strain curve fatigue performance, which can estimate safety life N_f.

Overall, the fatigue test of 3D printed materials for laboratory equipment requirement is complex, may test a long time, and there are no standard fatigue test for 3D printed ABS to follow, and therefore less current research. Further, during the fatigue test results of the experimental frequency vulnerable to cyclic loading, many factors affect the polymer molar mass, orientation, temperature and other experiments, the conditions difficult to control, thus poor reproducibility of the experiment.

6. CONCLUSIONS AND RECOMMENDATIONS

6.1 Summary

In this research, an ASTM standard tensile test is presented on 3D printed ABS tensile bar. The dumbbell-shaped specimen was printed on Stratasys printer. Tensile analyses are performed by pulling a constant force on one side and fixed the other side. The procedure was demonstrated by preforming tensile analysis on ASTM D638 Type IV. In addition, a computer based analysis was performed by using ANSYS finite element software, simulation of ASTM D638 model under force displacement loads and thus to plot the tensile stress-strain curves of samples. Also, creep test was conducted on 3D printed bar with three different printing angles. Through the creep test, which put a material under a constant temperature and constant stress for a long time to observe the occurrence of slow plastic deformation behavior, creep limit of each printing orientation was found. Last but not least, by conducting fatigue experiment, an S-N curve has been measured. The establishment of the curve and its corresponding stress amplitude with cycle shows how stress value determines the specimen can withstand a number of stress cycles without breaking.

During the tensile and creep test, the specimen geometry and the mechanics of test machines can impact the test results. Therefore, this test has sought a load axis, which consistent with the testing machine geometric center axis, in order to avoid offset tension during trials. Different restraint conditions at the end of the specimen, the stress distribution of the specimen will be dissimilar. However, when the specimens crack, if the end of the test piece is free to rotate, and even if the geometry of the test piece can still be assured, the stress distribution of the test piece has changed. Different end constraints on the specimen can affect tensile test results. Compared with the end portion of the tensile specimen freely rotate, the presence of

the end restraint specimens under normal circumstances, can result higher the peak value of the stress and strain. This indication can be observed in the chapter of ANSYS analysis.

In a uni-axial fatigue test, when the test piece using the same model as Terco standard, can obtain more uniform static fracture in the middle of the specimen with a long test period interval. Tensile load can be passed by loading the specimen with spring. Due to springs mechanical load, the specimen experiencing a uni-axial stress, the grip portion is tough to fracture, stress-strain curve can be obtained and experimental error is small. Increasing the mechanical load at the end of the specimen can fracture the middle of the specimen faster, also the cross-section of specimens will show a large amount static fracture concentration. If the specimen has large voids or gaps, so the stress distribution is less uniform, results more experimental error. By using cylindrical specimens, it will deliver the most uniform stress distribution, and the test results are most stable.

6.2 Conclusions

Based on the physical and simulated tests in this research, the following conclusions can be made:

1. 0 ° printing orientation shows the best tensile properties among 0 °, 45 ° and 90 °.

2. Simulated tensile test and measured results agree with each other in elastic region, which confirmed the reasonableness of analog design parameters.

3. In physical tensile test, 0 ° printing orientation has largest Youngs modulus and ultimate strength, results on average at 1.81 GPa and 224 MPa respectively.

4. During the creep test, the 90 ° printing orientation has the lowest k values, which is around 0.2, and shows the best creep properties among 0 °, 45 ° and 90 °.

5. Based on the fatigue data approximating equation, the values of A and B from test average and the linear least-square fitting results relatively agree.

6. During the fatigue test, the average cycle number under the load of 30N is 3796 revolutions. The average cycle number decreased to 128 revolutions when the load is 60N.

7. Despite the increasing cycle number with large amount of load, surprisingly small differences in the crack length can have a large effect on the crack growth rate. Therefore, when choosing the printing parameter, 100% infill would result lower fatigue crack growth rates.

8. Compare the stress level in tensile and fatigue test, has a large amount of difference at N_f equals to 1, due the different strain rate and model dimension.

6.3 Recommendations

Based on the research accomplished in this thesis, some recommendations are:

1. In this research, only elastic analysis has been conducted; a plastic model study will show the tensile property under a large amount of load.

2. A non-contact strain gauge can be used in the future tensile test, in order to increase measuring accuracy, and a provide more precise strain rate.

3. The fatigue test machine will need re-balance, in order to increase the loading accuracy.

4. If further creep experiments will be done in the future regarding the 3D printed model, the loads should be varied. This will give even a better understanding of the ABS material and will help with finding constant B and m.

LIST OF REFERENCES

LIST OF REFERENCES

[1] H. Lipson and M. Kurman, *Fabricated: The new world of 3D printing.* John Wiley and Sons, 2013.

[2] K. K. Reichl and D. J. Inman, *Dynamic Modulus Properties of Objet Connex 3D Printer Digital Materials*, pp. 191–198. Springer, 2016.

[3] L. Li, Q. Sun, C. Bellehumeur, and P. Gu, "Composite modeling and analysis for fabrication of fdm prototypes with locally controlled properties," *journal of Manufacturing Processes*, vol. 4, no. 2, pp. 129–141, 2002.

[4] V. Schppner and K. P. KTP, "Mechanical properties of fused deposition modeling parts manufactured with ultem 9085,"

[5] E. J. McCullough and V. K. Yadavalli, "Surface modification of fused deposition modeling abs to enable rapid prototyping of biomedical microdevices," *Journal of Materials Processing Technology*, vol. 213, no. 6, pp. 947–954, 2013.

[6] T. Letcher and M. Waytashek, "Material property testing of 3d-printed specimen in pla on an entry-level 3d printer," in *ASME 2014 International Mechanical Engineering Congress and Exposition*, vol. 2A, pp. 14–22, American Society of Mechanical Engineers.

[7] S. El-Gizawy, S. Corl, and B. Graybill, "Process-induced properties of fdm products," technical report.

[8] F. Rayegani and G. C. Onwubolu, "Fused deposition modelling (fdm) process parameter prediction and optimization using group method for data handling (gmdh) and differential evolution (de)," *The International Journal of Advanced Manufacturing Technology*, vol. 73, no. 1-4, pp. 509–519, 2014.

[9] "Standard test methods for flexural properties of unreinforced and reinforced plastics and electrical insulating materials," in *ASTM Subcommittee D20. 10 on Mechanical Properties*.

[10] M. S. Hossain, J. Ramos, D. Espalin, M. Perez, and R. Wicker, "Improving tensile mechanical properties of fdm-manufactured specimens via modifying build parameters," in *International Solid Freeform Fabrication Symposium: An Additive Manufacturing Conference. Austin, TX*, vol. 2013, pp. 380–392.

[11] L. Cai, H. Zhang, P. Byrd, K. Schlarman, Y. Zhang, M. Golub, and J. Zhang, "Effect of printing orientation on strength of 3d printed abs plastics," in *TMS 2016: 145 Annual Meeting and Exhibition: Supplemental Proceedings*, pp. 199–204, John Wiley and Sons, Inc.

[12] J. T. Belter and A. M. Dollar, "Strengthening of 3d printed fused deposition manufactured parts using the fill compositing technique," *PLoS ONE*, vol. 10, no. 4, p. e0122915, 2015.

[13] P. Brindley and R. Goodridge, "Preliminary investigation into the mechanical properties of stratasys polycarbonate and m30 abs materials," technical report, www.stratasys.com, 2008.

[14] B. Tymrak, M. Kreiger, and J. M. Pearce, "Mechanical properties of components fabricated with open-source 3-d printers under realistic environmental conditions," *Materials and Design*, vol. 58, pp. 242–246, 2014.

[15] A. Bagsik, V. Schppner, and E. Klemp, "Fdm part quality manufactured with ultem 9085," in *14th International Scientific Conference on Polymeric Materials*, vol. 15, pp. 307–315.

[16] R. Sayre III, *A Comparative Finite Element Stress Analysis of Isotropic and Fusion Deposited 3D Printed Polymer*. Master's Thesis, Rensselaer Polytechnic Institute, 2014.

[17] B. Banerjee, J. Chen, and A. Kathirgamanathan, "Comparison of ansys elements shell181 and solsh190," 2011.

[18] A. Ahmad, S. Darmoul, W. Ameen, M. H. Abidi, and A. M. Al-Ahmari, "Rapid prototyping for assembly training and validation," *IFAC-PapersOnLine*, vol. 48, no. 3, pp. 412–417, 2015.

[19] N. E. Dowling, *Mechanical behavior of materials : engineering methods for deformation, fracture, and fatigue*. Boston: Pearson, 2013.

[20] J. Lee and A. Huang, "Fatigue analysis of fdm materials," *Rapid Prototyping Journal*, vol. 19, no. 4, pp. 291–299, 2013.

[21] "Mechanical design 2*nd*, fatigue experimental lab," instruction manual, IUPUI Mechanical Engineering Department, 2007.

[22] J. P. Moore and C. B. Williams, "Fatigue properties of parts printed by polyjet material jetting," *Rapid Prototyping Journal*, vol. 21, no. 6, pp. 675–685, 2015.

[23] M. Ciavarella and N. Pugno, "A generalized parislaw for fatigue crack growth," *Associazione Italiana per lAnalisi delle Sollecitazioni. XXXIV. Politcnico de Milano*, 2005.

PUBLICATIONS

PUBLICATIONS

1. Jing Zhang, Yi Zhang, Hanyin Zhang, Michael Golub, Comparative Study of Mechanical Properties of 3D Printed Plastic Components, Materials Science and Technology 2016 (MS&T16), Salt Lake City, UT, USA, October 23-27, 2016
2. Weijie Zhang, Hanyin Zhang, Alycia Berman, Xinyao Hu, Jiayang Liu, Zaixin Feng, Tien-Min Gabriel Chu, Jing Zhang, Electrochemical Study of Biocompatible Magnesium Alloys, IUPUI Research Day, Indianapolis, IN, April 5, 2013
3. Jing Zhang, Weijie Zhang, Zhuoyi Jiang, Hanyin Zhang, Yuanjun Guo, Chengyun Ning, Study of Residual Stress in Pulsed DC Microarc Oxidation Coatings on Biocompatible AZ31 Magnesium Alloys. Materials Science and Technology 2012 Conference and Exhibition, October 7-11, 2012, Pittsburgh, PA
4. Weijie Zhang, Zhuoyi Jiang, Hanyin Zhang, Jing Zhang, Residual Stress Analysis of Ceramic Coatings on Biocompatible Magnesium Alloys, IUPUI Research Day, Indianapolis, IN, April 13, 2012